

## RESEARCH ARTICLE

# Structurally informed design of interlocking block assemblages using limit analysis

Elham Mousavian\* and Claudia Casapulla

Department of Structures for Engineering and Architecture, University of Naples Federico II, via Forno Vecchio 36, 80134 Naples, Italy

\*Corresponding author. E-mail: [elham.mousavian@unina.it](mailto:elham.mousavian@unina.it)

## Abstract

This paper presents a computational framework to design assemblages of interlocking blocks and to analyze their structural feasibility. The core of this framework is an extension of limit analysis to corrugated interfaces with orthotropic sliding behavior. Such block interfaces are made of a number of locks (i.e. projections on the corrugated faces, locking the blocks together) with rectangular cross section. The sliding resistance at the block interfaces is governed by the shear resistance of the locks and Coulomb's friction law, normal to and along the locks, respectively. This resistance is assumed as a function of different interface geometric parameters and the stress state on an interface is represented by using a number of contact points distributed over the lock centerlines. The abstraction model has been validated through the comparison of the torsion–shear behavior of an interface obtained by the proposed model and experimental tests reported in the literature. The extended limit analysis has been implemented to model single-layer shells. When the model is infeasible, the geometry of the overall shell, blocks, and interlocking interfaces can be adjusted by the designer to make the model structurally feasible. The performance of the framework is presented through several examples, which demonstrate the relationships between the geometry of the interlocking interfaces and the stability of the assemblages.

**Keywords:** limit analysis extension; orthotropic sliding resistance; interlocking masonry blocks; computer-aided conceptual design; structurally informed design

## 1. Introduction

Digital tools for structurally informed architectural design have been introduced from the early 1990s, within the framework of computer-aided design. Yet, the interaction of the designers and the digital tools to improve the designers' creativity at the early stages of design is a new topic (Zboinska, 2019). Among various structural systems, there are several tools to design structurally informed compression-only buildings, including masonry assemblages. These tools show an architect in real time whether his/her design is structurally feasible so that he/she can adjust the design parameters (Lee, Van Mele, & Block, 2016), or automatically tune the parameters to make an infeasible model stable (Block & Lachauer, 2011; Whiting, Ochsendorf, & Durand, 2009). The applied structural methods to develop such tools must be computationally efficient still highly accurate, in order to make the fast shape exploration possible during the early stages of design.

The limit analysis method using thrust line (Harvey, 1988; Heyman, 1995), thrust network (Block, 2009; O'Dwyer, 1999), membrane (D'Ayala & Casapulla, 2001; D'Ayala & Tomasoni, 2011), and similar approaches reviewed by Rippmann (2016) has been implemented to design single-layer shells. Algebraic graphic statics used to construct thrust lines was also applied to design 2D compression-only

Received: 19 November 2019; Revised: 14 January 2020; Accepted: 20 January 2020

© The Author(s) 2020. Published by Oxford University Press on behalf of the Society for Computational Design and Engineering. This is an Open Access article distributed under the terms of the Creative Commons Attribution Non-Commercial License (<http://creativecommons.org/licenses/by-nc/4.0/>), which permits non-commercial re-use, distribution, and reproduction in any medium, provided the original work is properly cited. For commercial re-use, please contact [journals.permissions@oup.com](mailto:journals.permissions@oup.com)

multilayer framed structures (Akbarzadeh, Van Mele, & Block, 2014) as well as truss structures with compressive and tensile bars (Van Mele & Block, 2014). It was further extended to design compression-only spatial structures using convex polyhedral force diagrams (Akbarzadeh, Van Mele, & Block, 2015; Lee, Van Mele, & Block, 2018).

Limit analysis introduced by Heyman (1995) is a well-known method to analyze masonry structures through abstracting an assemblage of rigid blocks to the interfaces at which internal forces are distributed. It is more computationally efficient than finite element analysis, including detailed and simplified models (Chisari, Macorini, Amadio, & Izzuddin, 2018; Li & Atamturktur, 2013; Lourenço, Rots, & Blaauwendraad, 1995; Olmati, Gkoumas, & Bontempi, 2019), and discrete element analysis (Bui, Limam, Sarhosis, & Hjiiaj, 2017; Cannizzaro, Pantò, Caddemi, & Calì, 2018). Despite some limitations to the related safe theorem (Bagi, 2014), its kinematic approach has also recently been used for the nonlinear static analysis of rocking masonry structures (Casapulla, Giresini, Argiento, & Maione, 2019), as a valid alternative to the dynamic analysis (Giresini, Sassu, & Sorrentino, 2018; Giresini, Solarino, Paganelli, Oliveira, & Froli, 2019). Concave and convex contact models within the limit analysis framework are two other approaches specifically suitable to analyze assemblages with different topologies (Casapulla & Maione, 2018; Frick, Van Mele, & Block, 2015, 2016; Livesley, 1978, 1992; Whiting, Ochsendorf, & Durand, 2009). In those models, the failure modes of interfaces are defined through constraining the internal forces at one (convexity formulation) or several contact points (concavity formulation). All the approaches introduced above considered flat interfaces with infinite (Heyman, 1995) or finite isotropic associative (Livesley, 1978, 1992) and nonassociative (Casapulla & Argiento, 2018; Gilbert, Casapulla, & Ahmed, 2006; Portioli, Casapulla, Gilbert, & Cascini, 2014) frictional resistances.

This work extends the limit analysis method with the concave contact model to the interlocking interfaces with nonisotropic sliding behavior. Objects with complex shapes (furniture, buildings, etc.) are usually partitioned into smaller units to simplify the manufacturing, transport, and assembling processes. Partitioning, however, may reduce the amount of the external force (load) the object can bear. Novel techniques such as additive manufacturing-oriented design try to remedy this situation by manufacturing the complex objects with no partition (Sossou, Demoly, Montavon, & Gomes, 2018). Still using interlocking interfaces is a classical but efficient way to keep the load-bearing capacity of the object the same after being discretized. The proper geometry for the interlocking interfaces is found according to various objectives, including manufacturability and assemblability (Fernando, Weir, Reinhardt, & Hannouch, 2019; Wang, Song, & Pauly, 2018) and structural function (Sassu, Giresini, Bonannini, & Puppio, 2016). Recently, several studies have been carried out on the structural behavior of interlocking interfaces with different geometries. Experimental and numerical tests (Hossain, Totoev, & Masia, 2016; Liu, Liu, Lin, & Zhao, 2016; Totoev, 2015) investigated the in-plane and out-of-plane capacity of masonry walls composed of blocks with corrugated interfaces. Out-of-plane behavior of osteomorphic blocks and interfaces with cross-shaped locks (locks are projections attached to the main body of the blocks, interlocking the blocks against sliding) was also experimentally investigated by Dyskin, Pasternak, and Estrin (2012), Dyskin, Estrin, and Pasternak (2019), and Ali, Gultom, and Chouw (2012). Similarly, experimental and numerical investigations were carried out on the different behavior of wooden joinery connections with different geometric properties (Fang & Mueller, 2018; Sassu, De Falco, Giresini, & Puppio, 2016).

The sliding behavior of the interfaces with corrugated shapes having locks with rectangular cross section is herein investigated. In this study, an interlocking interface is equated to a flat interface with orthotropic sliding resistance where the interface sliding behavior normal to and along the locks is governed by the shear resistance of the locks and Coulomb's friction law, respectively. In this case, the sliding resistance is a function of the geometric properties of the locks, including their orientation and width. It is worth highlighting that associated flow rules (friction with dilatancy) for sliding along the locks are assumed within this extended limit analysis, while solutions with nonassociated flow rules can be accommodated by adopting the iterative procedure proposed by Gilbert, Casapulla, and Ahmed (2006).

In the following, the concave contact model for the interlocking interfaces is first introduced in Section 2. Section 3 demonstrates the developed computational framework for a structurally informed design of single-layer shells composed of interlocking blocks, in which the extended concave contact model was implemented. Examples modeled and analyzed using this framework are presented in Section 4. Finally, the conclusions are outlined.

## 2. Concave Contact Model for Interlocking Blocks

In this section, the proposed concave contact model for interlocking interfaces is first described and then validated.

As introduced earlier, according to the pioneering discrete element approach (Heyman, 1995; Kooharian, 1952), a system of rigid blocks with dry joints can be considered as an assemblage of discrete elements and contact interfaces between them. These contact interfaces are, in fact, the potential failure planes on which the internal forces are distributed. To build the structural model with interlocking blocks, the possible failure planes are first determined. The structure is then modeled as an assemblage of rigid bodies with these failure planes as their boundaries.

For an interlocking interface sketched in Fig. 1a, the failure planes are assumed to be the “dry joints” between two interlocking blocks (blue strips), together with the “fracture planes” at which each block might crack (red strips) (Fig. 1b). The main body of the interlocking block is assumed rigid enough so that other types of potential fracture planes are avoided, e.g. by considering it stocky enough.

The dry joints only rock/separate when the normal forces on them are in tension or slide along the direction parallel to the locks when violating the Coulomb's friction constraint. The fracture planes slide or twist when the shear or torsion yielding conditions are reached, respectively. It is worth noting that when an interface is only subjected to pure shear normal to the locks, one of the two side locks does not resist the shear stresses, and therefore its joint to the main body of the block does not act as a fracture plane (Fig. 1c). However, the direction of the lateral force is not a pre-known input parameter and can be obtained by finding the flow of forces on an assemblage during the structural analysis. Therefore, for both pure shear and torsion-shear failures, all the planes at which the locks are connected to the main body of the block are considered as fracture planes.

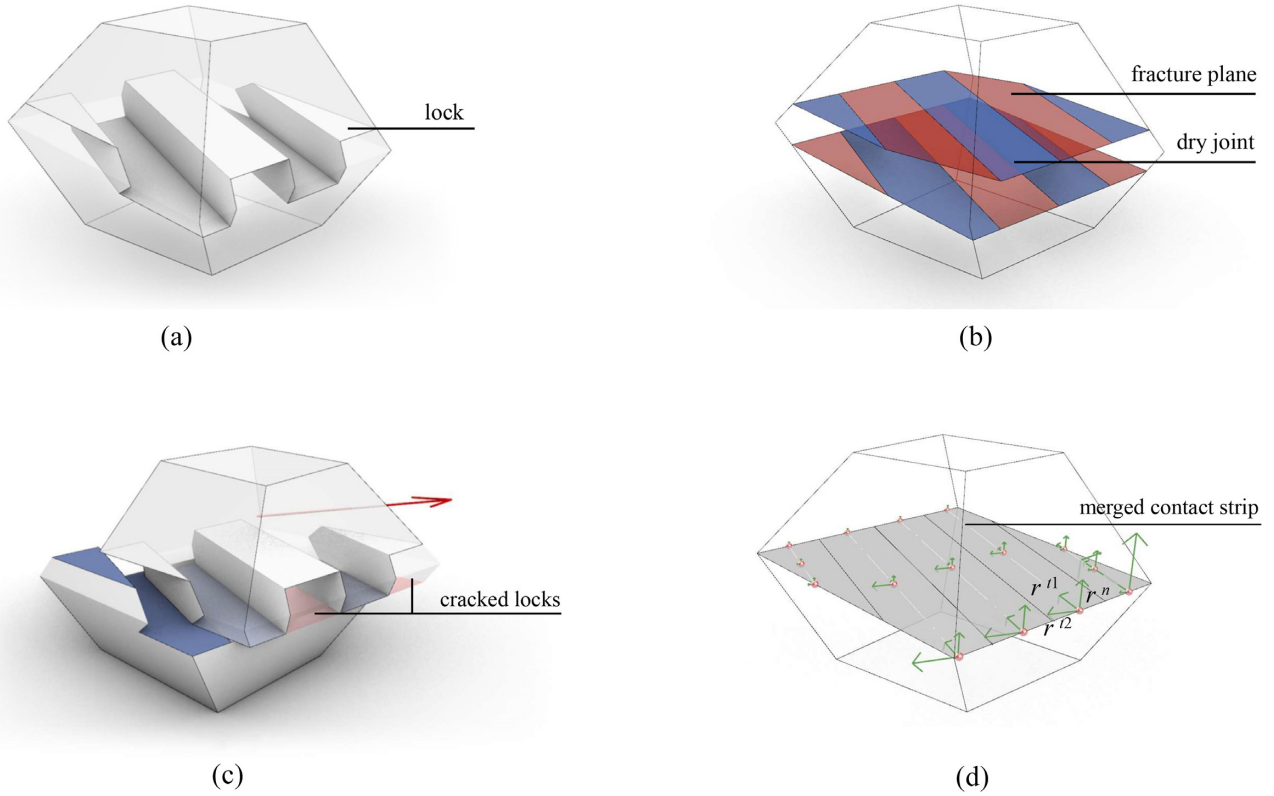


Figure 1: (a) Two interlocking blocks kept together by the locks on the shared interface; (b) dry joints (blue strips) and fracture planes (red strips), at which failure may occur; (c) cracked locks when the interface is only subjected to pure shear normal to the locks; and (d) merged strips and contact points distributed on their CLs.

To simplify the model of the stress state on the contact interfaces, the fracture and dry joint contact strips belonging to an interlocking interface are merged. The concave contact model assumes that by finding the internal forces at some points on a contact interface and assigning limiting values to those forces, the structural behavior of this face can be estimated. The classical approach with the concave contact model developed by Livesley (1992) for conventional blocks considers a model structurally feasible when (i) all the internal forces at the contact points of an individual block are in equilibrium with the external forces and torques imposed on that block centroid; (ii) the normal components of the internal forces are in compression; and (iii) the two perpendicular tangential components of the internal forces must satisfy the sliding constraints according to the Coulomb's friction law.

To extend this model to the interlocking interface, a number of points are distributed over the centerline (CL) of any merged strip representing a lock (Fig. 1d). The logic behind this point distribution is explained in the following section. In fact, seven options for the contact point distribution on every lock CL are analytically tested to check which one may better represent the sliding behavior at the interlocking interface.

Three limiting conditions for the internal force at every contact point are assumed as follows: (i) the normal component of the internal force ( $r^n$ ) must be in compression; (ii) the tangential component of the internal force parallel to a lock ( $r^{t1}$ ) must satisfy the Coulomb's friction law; and (iii) the tangential component of the internal force normal to a lock ( $r^{t2}$ ) must be less than the torsion-shear resistance at that point (Fig. 1d). This torsion-shear resistance is a portion of the pure shear resistance of a fracture strip between a lock and the main body of the block when it is subjected to uniformly distributed tangential forces. How this resistance is computed is explained in the following section.

### 2.1. Torsion-shear resistance of a fracture strip

In the proposed concave formulation, each lock is idealized as a linear component at its CL (Fig. 2a and b). The tangential forces (normal to the CL) are distributed on the lock CL, uniformly (when related to the pure shear failure at the interface, Fig. 2c) or nonuniformly (when related to the mixed torsion-shear failure, Fig. 2d), so that

$$f(b) \leq f_y, \quad (1)$$

where  $f(b)$  and  $f_y$  are the tangential force as a function of  $b$  and the shear resistance per unit length of the lock CL, respectively. In this paper, it is simply assumed  $f_y = (\tau_k s)$ , where  $s$  is the lock thickness and  $\tau_k$  is the material shear strength (e.g. cohesion for a cohesive material). A slightly different assumption was considered for  $f_y$  in a previous paper dealing with interlocking blocks (Casapulla, Mousavian, & Zarghani, 2019), and experimental tests on the torsion-shear behavior of a lock attached to the main body of a masonry block are under development to validate the actual value. However, the most conservative shear resistance due to the absence of normal forces is considered in this analysis.

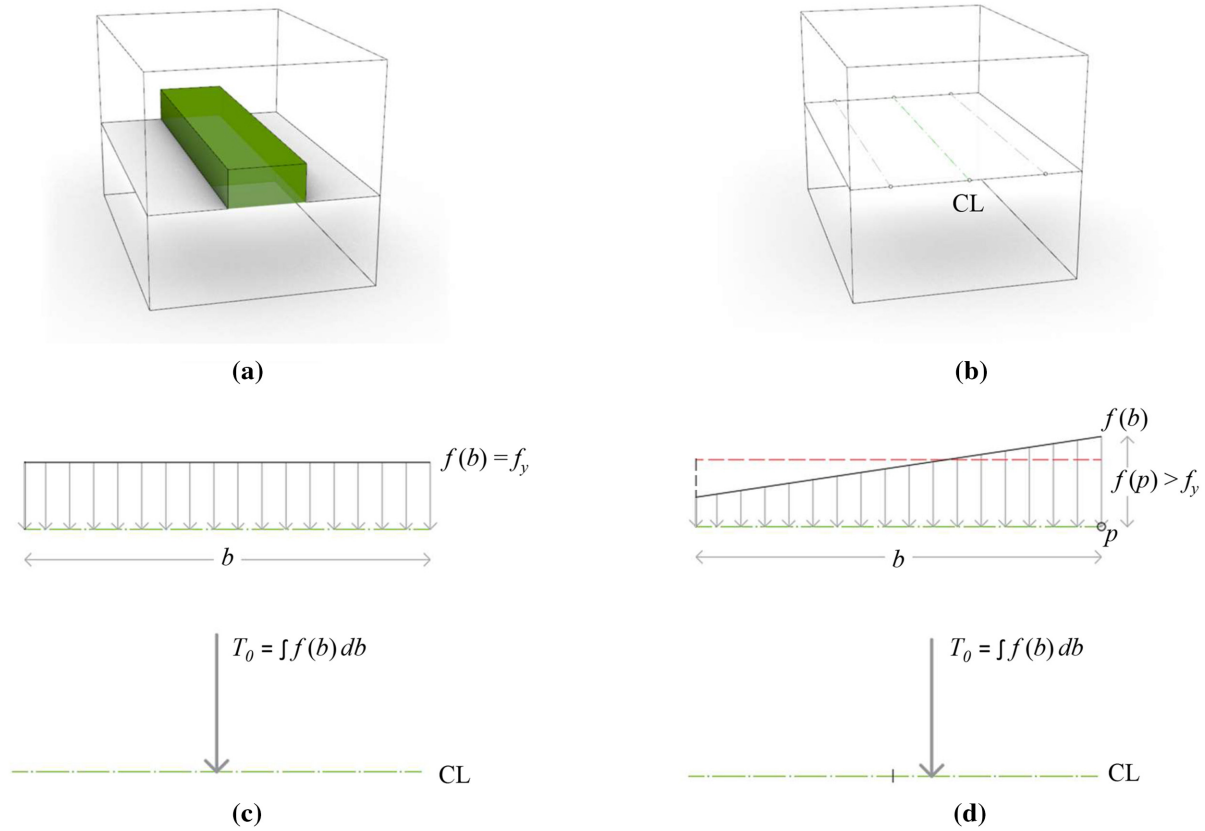


Figure 2: (a) The generic lock; (b) the CLs of the fracture planes between the locks and the main bodies of the blocks; and (c) uniform and (d) infeasible nonuniform distributions of the tangential force on the lock CL and their resultants.

When the tangential forces are uniformly distributed along the lateral face of the lock, both sides of equation (1) can be multiplied by the lock length  $b$ , so that  $f_y b$  represents the pure shear resistance denoted by  $T_0$ . This is the tangential resistance at the fracture plane when only shear stress and no torsion exist.

Assuming that the resultant of the nonuniformly distributed forces is a combination of shear and torque applied at the midpoint of the lock CL, the yielding value of the shear force  $T_r$  should be less than  $T_0$ ; i.e. the shear resistance at the fracture plane (which equals  $T_r$ ) is smaller than  $T_0$ . The reason is that when nonuniformly distributed force with the resultant equal to  $T_0$  (pure shear resistance) is applied to a lock, there is at least one point at which  $f(b) \geq f_y$  (Fig. 2c and d). Casapulla and Maione (2018) demonstrated the inverse correlation between the yielding values of these shear force and torsion.

To reproduce the torsion-shear resistance of a lock by using the concave contact model, the forces distributed over the lock CL are substituted by some point loads. The shear force at each contact point  $i$  must be less than  $T_0$  and can be expressed as a portion of  $T_0$  through a weight  $p_i$ , so that  $\sum_{i=1}^n p_i = 1$ .

Seven options for distributing the contact points (number and location of the points) and weighting the shear resistance at the points are herein tested to find the closest option to the real torsion-shear behavior of the fracture plane, similarly to that developed by Lemos (2017). In four options, two points are located at 0, 1/6, 1/4, and 1/3 distance from the endpoints of the lock CL (options 1–4 in Fig. 3a). The shear resistance at each point is  $T_0/2$ . In other three options, three points are located at the endpoints and the midpoint of the lock CL. The shear resistances at these points are displayed in Fig. 3b.

In order to find the best option, the yielding torsion and tangential force for each of the options are compared to those obtained by the convex formulation and the experimental test described by Casapulla and Portioli (2015). That experiment was carried out on two stacked tuff blocks, of which the upper one was subjected to a lateral horizontal force with different eccentricities and the lower one was completely fixed. Applying a large overload on the upper block, this could only slide/twist. For different values of eccentricity, the yielding amount of tangential force, by which the upper block started to slide/twist, was recorded.

The same test is herein analytically reproduced on two dry-stacked rigid units with a corrugated interface (Fig. 4). Each unit is composed of a rigid main body and two rigid locks, while cohesive material with quasi-brittle behavior is assumed between the main body and each lock. The interface between the units is assumed to be a fracture plane, for which the pure shear resistance is considered similar to the pure sliding resistance of the dry joint between the stacked tuff blocks experimentally tested. In particular, the following assumptions are also made:

- The units are modeled with the same dimensions and weights of the tuff blocks tested by Casapulla and Portioli (2015).
- The same amount of overload avoiding rocking is also applied at the centroid of the upper unit.

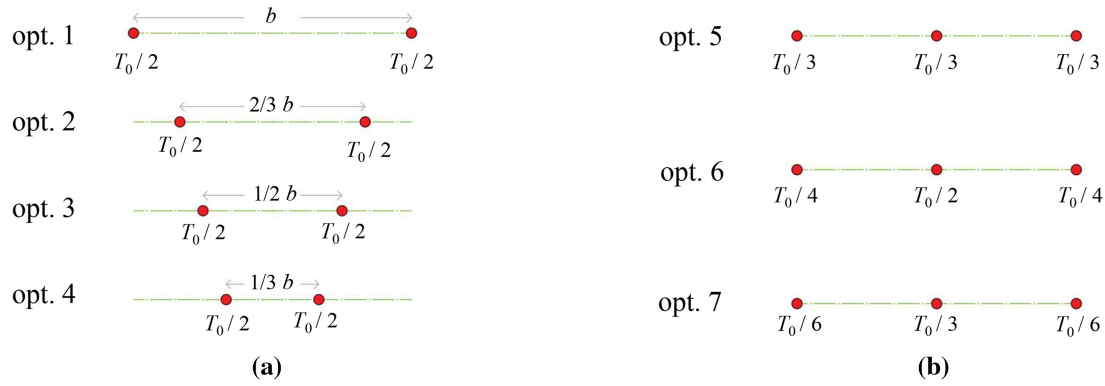


**Figure 3:** Shear resistance at each point on the CL of a fracture strip between the lock and the main body of the block in the proposed concave model: (a) four options for two contact points and (b) three options for three contact points.

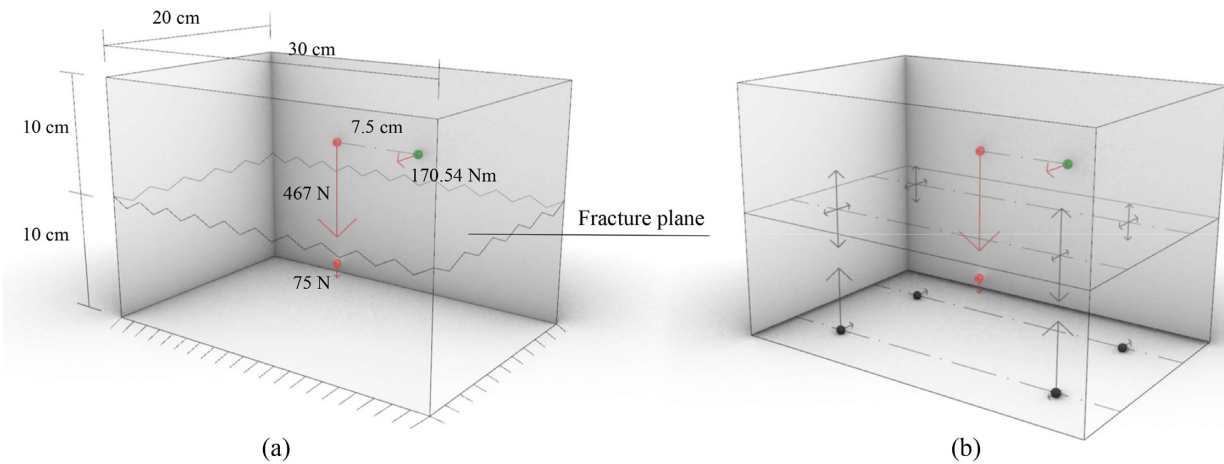


**Figure 4:** (a) A setup of two stacked blocks to study the torsion–shear interaction at the interface (Casapulla & Portioli, 2015) and (b) yielding state of the concave model—option 2 for 7.5 cm eccentricity of the lateral force. Green and black points show the eccentric force application point and the supports, respectively.

- A lateral force and a torsion moment are applied at the centroid of the upper unit. The amount of the torsion moment is equal to the product of the lateral force and the eccentricity.
- The interface is abstracted by two CLs on which the contact points are distributed. The assumption of one CL is not possible since the model subjected to the lateral force normal to a single CL cannot be equilibrated. The internal force on the interlocking interface equilibrating the external force passes through the intersection of the interlocking interface and the external force trajectory. This intersection point can be located outside of a single CL located on the interface midline. In this case, no equilibrating internal force can be found at the contact points on this CL. Considering two CLs for the interlocking interface, finding the internal forces equilibrating the external force is possible.
- While at point  $i$ ,  $|r_i^{t2}| \leq p_i T_0$ , the sliding resistance along the CLs is considered to be zero, i.e.  $r_i^{t1} = 0$ .

Figure 5 shows different curves demonstrating the interaction of yielding torsion moment and tangential force for experimental results (Casapulla & Portioli, 2015) (black dots), the convex method presented by Casapulla and Portioli (2015) (red dashed curve), and the proposed options 1–7. The figure also shows that the closest graph to the result of the experimental test and convex model is option 5. Among the models with two contact points on a CL, option 2 has the best agreement, yet providing conservative results.

### 3. Computational Setup

The limit analysis method for interlocking blocks, described in Section 2, is herein implemented to develop a plug-in for grasshopper (GH) editor, using C# programming language, with reference to the design of a single-layer shell composed of interlocking blocks. This section first introduces an overview of the design process outlined for this plug-in, including the parametric modeling and the structural analysis phases. Then, the modeling elements and data structures organizing the elements are introduced, and the concave contact model extended to interlocking interfaces is adopted and formulated.



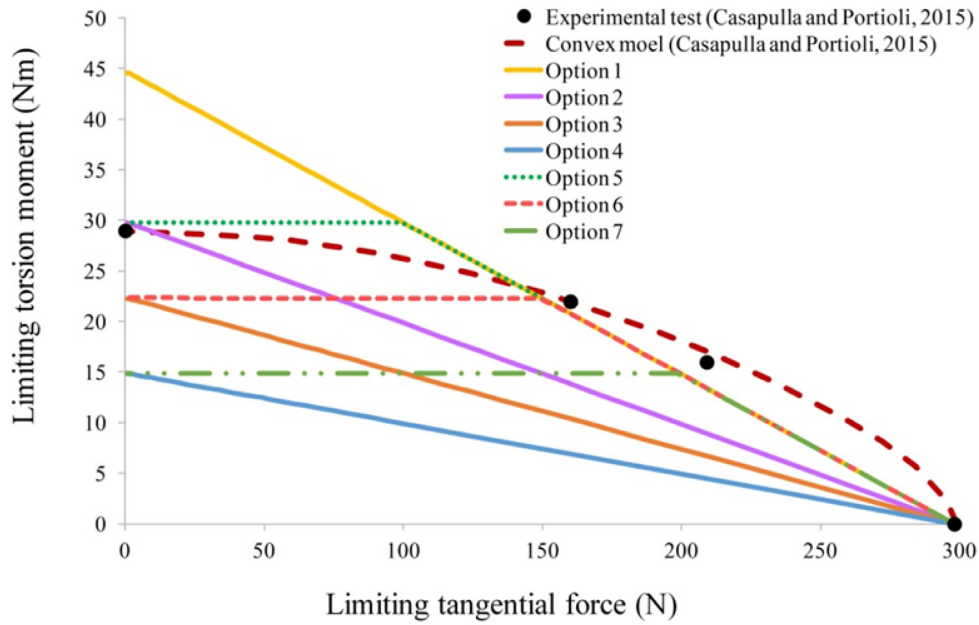


Figure 5: Yielding torsion–shear interaction for seven options of the proposed concave model, and the convex model and the experimental test described by Casapulla and Portioli (2015).

### 3.1. Design process

The plug-in consists of five custom GH components for (i) modeling the overall shell and its rigid blocks, (ii) modeling the interlocking interfaces, (iii) determining the boundary conditions, (iv) defining the external forces and torques, and (v) analyzing the structural feasibility of the designed model. The design workflow using these GH components is demonstrated in Fig. 6. In the following two sections, each component is introduced in detail.

### 3.2. Modeling phase

The framework is developed to design the single-layer assemblage of interlocking blocks propagated with a grid shape (stack bond) pattern. The main body of each block is a hexahedron unit and must have flat faces. Each grid line on the outer and inner faces of the assemblage consists of a set of block edges forming a polygonal chain (polyline), whose vertices are the corners of the blocks.

The gridlines are classified into two series of  $u$  and  $v$  polylines (Fig. 7a). The assemblage can be closed along a  $v$  gridline to model shapes such as cylinder, and can be converged toward the apex of the assemblage to form shapes like a dome with the radial grid (Fig. 7b).

#### 3.2.1. Modeling an assemblage of blocks

Given the outer and inner surfaces of a shell (extrados and intrados), which can have different geometries, a single-layer shell can be modeled. Then, given the data trees of the block corners on each surface as an input, an assemblage of blocks with a stack bond is formed. Through this GH component, the main bodies of the blocks are modeled. The interlocking interfaces are then modeled using another component shown in the next section. The block corners at each of the inner and outer surfaces are the intersection points of the  $u$  and  $v$  gridlines. Data tree of the block corners for each surface includes a number of primary branches denoted by  $b$ , so that branch  $b_i$  consists of the block corners over the  $i$ th  $v$  gridline denoted by  $p$  (Fig. 8).

The modeled assemblage of blocks includes four data trees organizing the block interfaces and a data tree of the block centroids as the output of the GH component. Following the classification of the gridlines to  $u$  and  $v$  types, the edges of the blocks are denoted by  $u$ ,  $v$ , and  $w$  (Fig. 9). Then, the block faces are called  $uv0$ ,  $uv1$ ,  $uw$ , and  $vw$ , which represent the block face on the outer and inner faces and the interfaces between the blocks in  $u$  and  $v$  directions, respectively. This arrangement allows extending the plug-in to model the multilayer assemblages; e.g. for an assemblage with  $l$  layers of blocks, the lock faces are organized as  $uv0$ ,  $uv1$ ,  $\dots$ ,  $uvl$  types. The data trees of the block centroids, and  $uv0$ ,  $uv1$ ,  $uw$ , and  $vw$  interfaces for the whole assemblage are organized with the same pattern of the input data trees of the block corners (Fig. 10).

In the following, items that should be considered by the designers to model a correct assemblage topology are listed. However, verifying the correctness of the assigned inputs by the framework and/or correcting them automatically are outside the scope of this paper. The list is as follows:

- The input data trees for the inner and outer surfaces of the assemblage must have the same number of elements.
- Two adjacent blocks must have a shared face, while only a shared corner or edge is not valid. As a result, the pattern of the grids on the outer and inner surfaces (open or closed) must be the same.

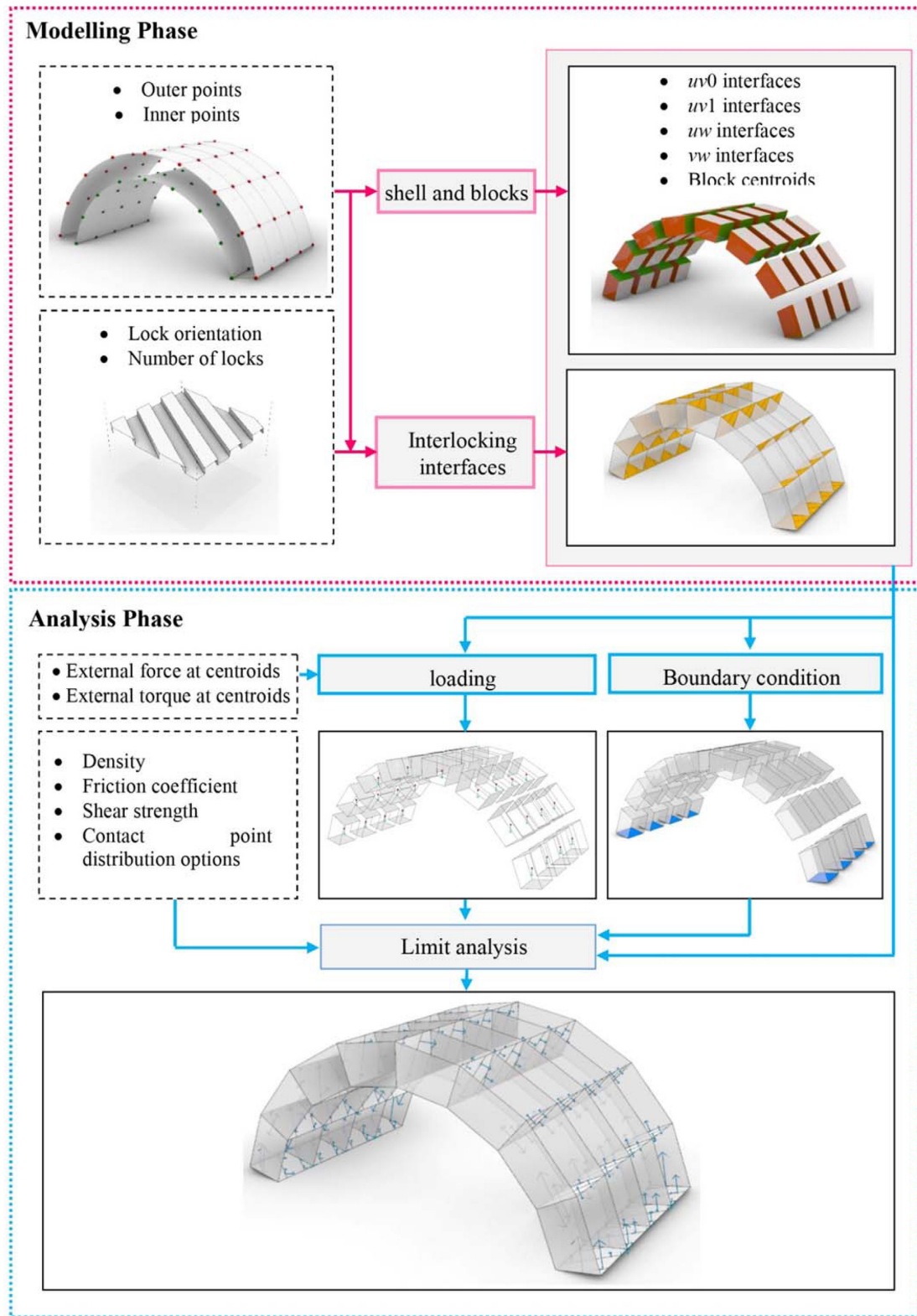


Figure 6: Design workflow. The inputs assigned by the designer are written in the boxes with black dashed frames.

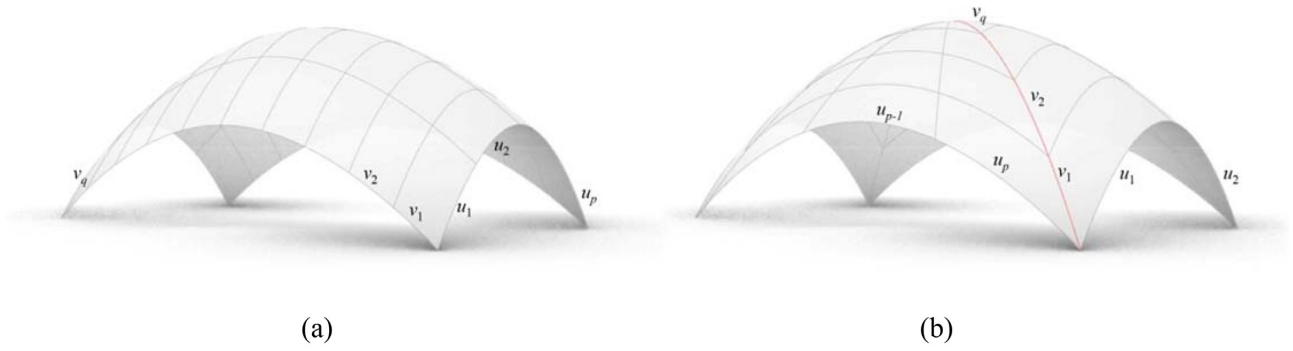


Figure 7: (a) Normal grid (stacked) and (b) radial grid bond pattern.

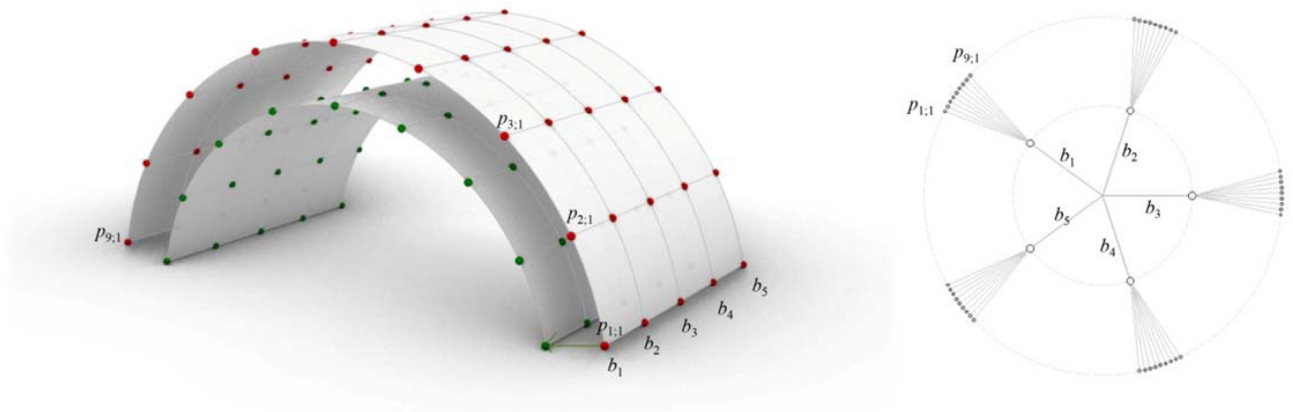


Figure 8: Two data trees to store the coordinates of the block corners on the outer and inner shells.

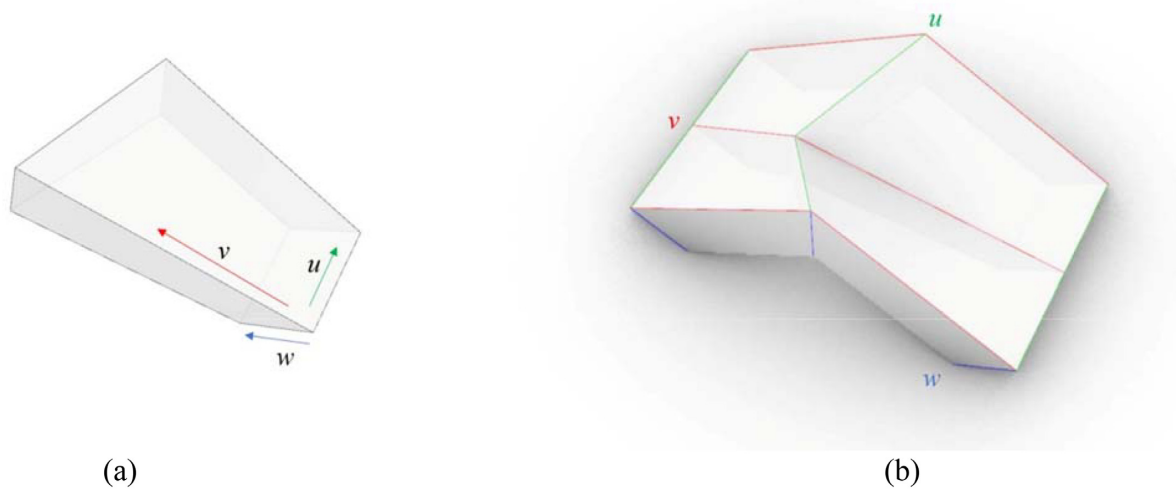


Figure 9: (a)  $u$ ,  $v$ , and  $w$  edges for a single block and (b)  $u$ ,  $v$ , and  $w$  gridlines for a whole shell with stack bond pattern.

- A key unit must be considered at the apex of the assemblages with a radial gridline to avoid modeling the blocks at the topmost row with only a shared vertical line. Currently, the framework is only able to model a hole (stands for a key unit with zero density).
- All the modeled block faces are convex flat quadrilaterals, whose edges have lengths more than zero. Flattening the curved faces will be regarded in further works.



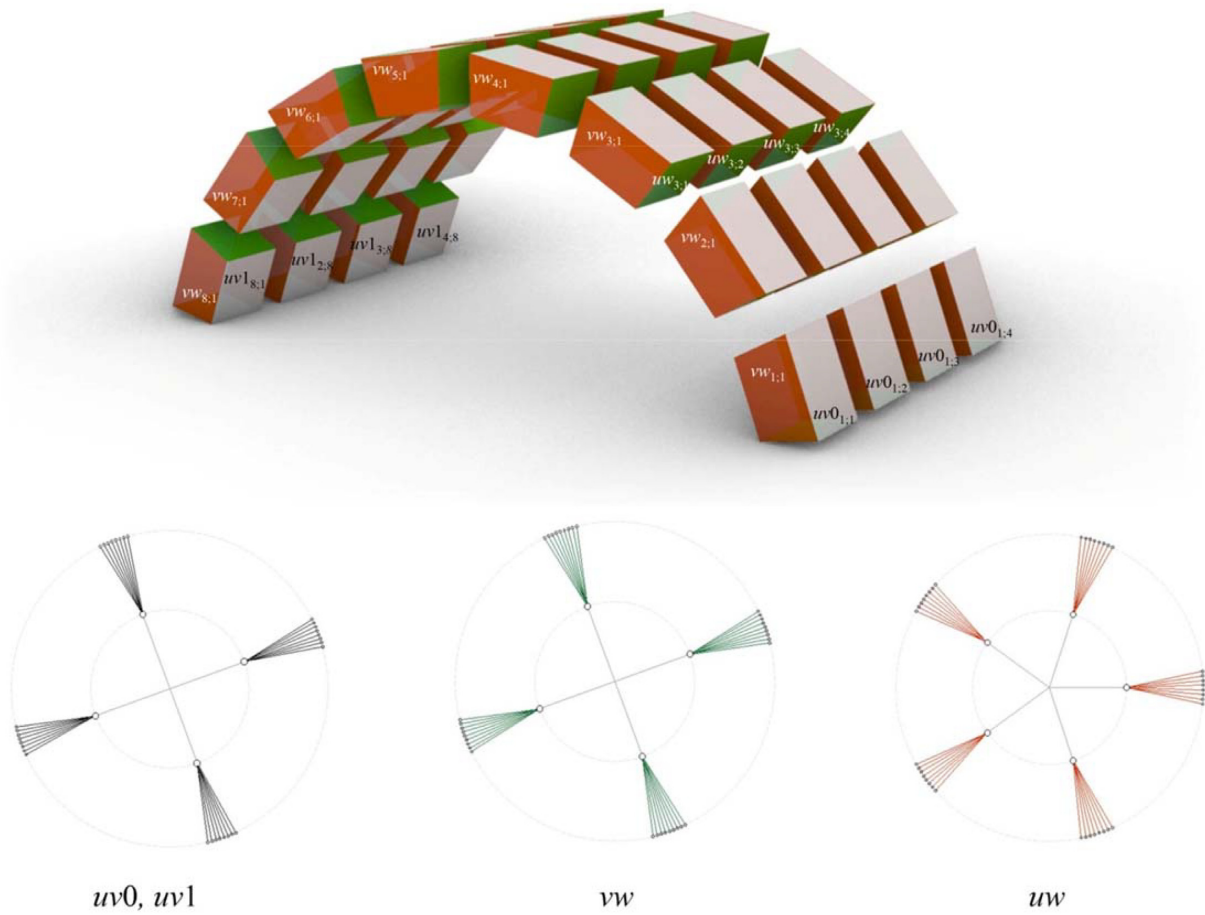


Figure 10: Data trees for four sets of interfaces  $uv0$ ,  $uv1$ ,  $vw$ , and  $uw$ .

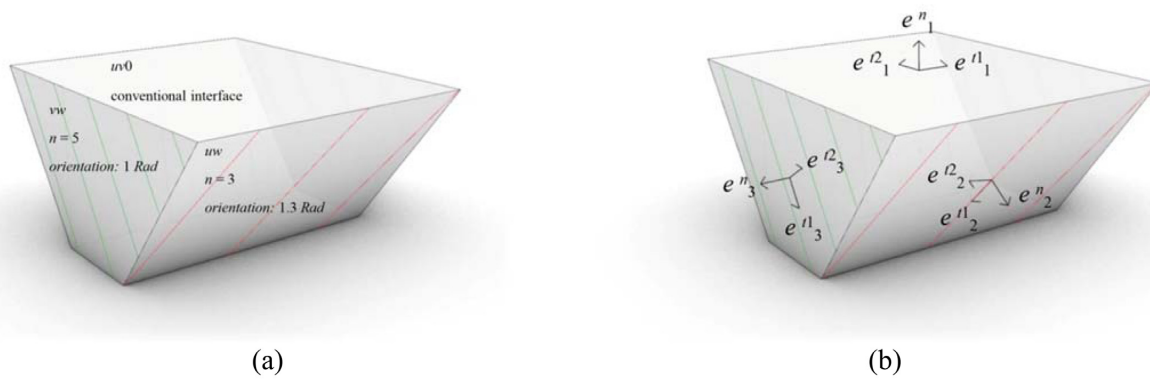


Figure 11: (a) Modeling of an interlocking interface and (b) unit local coordinates for each interface.

### 3.2.2. Modeling the interlocking interfaces

Interfaces produced by the first GH component (for an assemblage of blocks) can be modeled as interlocking interfaces using four GH components to make  $uv0$ ,  $uv1$ ,  $uw$ , and  $vw$  interface interlocking types. Otherwise, the interfaces are regarded as conventional flat type.

As in the first GH component, the inputs are the data trees of the block corners on outer and/or inner block surfaces, together with the number of locks and the orientation of locks with respect to a chosen edge of an interface. Each of these parameters can be modified during the interactive shape exploration. The output of each GH component is a data tree of the CLs of the locks on the interfaces (Fig. 11a).

### 3.3. Analysis phase

The limit analysis method with the concave contact model for interlocking interfaces, explained in Section 2, is formulated as a linear system of equation and implemented in the plug-in. To exploit the analysis, the loading and boundary conditions are first assigned through two GH components. Then, the modeled assemblage is analyzed by the final custom GH component.

#### 3.3.1. Boundary conditions

The designer must assign the boundary conditions. Supports should be chosen among the interfaces located on the external surfaces of the assemblage, including all the  $uv_0$  and  $uv_1$  interfaces and  $uw$  and  $vw$  interfaces located on the outer face of the shell. A GH component is developed to show the indices of the potential supports among the 1D flattened data trees of the interfaces (Section 3.2.1). For the  $i$ th face on the  $m$ th branch of a data tree with  $n$  faces, the face index in a flattened set is  $(m + 1)n + i$ . The designer can then select the desired indices among the potential supports.

#### 3.3.2. Loading conditions

An external force and an external torque with arbitrary values and directions can be imposed on the centroid of each block. A 3D vector defines each of them. The data tree collecting the block centroids (Section 3.2.1) is flattened as a 1D array so that for the  $i$ th block centroid on the  $m$ th branch, when each branch has  $n$  block centroid, the block centroid index is  $(m + 1)n + i$ . Forces and torques applied to the block centroids are then determined as two separated 1D arrays. For the block centroid with no external load and force, all elements of the assigned vector are zero.

In addition to the external forces and torques assigned by the designer, the weight of the blocks is automatically computed through the multiplication of the material density assigned by the designer and the hexahedron block volume.

#### 3.3.3. Limit analysis

Finally, the structural feasibility of the modeled block assemblage is analyzed by a GH component, whose inputs can be categorized into three groups:

- (i) Geometric inputs: the modeled assemblage built through two data trees of the block corners on the inner and outer surfaces of the assemblage, and the modeled interlocking interfaces in the form of the data trees collecting the CLs of the locks on the interfaces.
- (ii) Structural inputs: boundary conditions through the indices of the selected supports; loading conditions by defining the external forces and torques applied at each block centroid.
- (iii) Material properties: the friction coefficient  $\mu$ , shear strength  $\tau_k$ , and the density  $\rho$  by which each block weight is calculated.

All the inputs can be modified parametrically. If the number of the blocks changes during the shape exploration, the indices of the potential supports and block centroids at which the external loads are applied will be updated. Then, the designer must update the desired boundary and loading conditions.

According to limit analysis, the linear equilibrium problem of the concave model under the limiting conditions (compression, friction, and shear constraints) is solved using least squares formulation:

$$\begin{cases} \text{objective function} \\ \min \frac{1}{2}(C_{eq} \cdot \vec{r} + \vec{E})^2 & \text{equilibrium equation} \\ \text{subject to} \\ \begin{cases} r_{i,j}^n \leq 0 & \text{compression constraint} \\ |r_{i,j}^{t1}| \leq \mu |r_{i,j}^n| & \text{friction constraint} \\ |r_{i,j}^{t2}| \leq p_{i,j} T_0 & \text{shear constraint} \end{cases} \end{cases} \quad \forall i \in \text{contact points on merged strip } j; \sum_{i=1} p_{i,j} = 1, \quad (2)$$

where  $C_{eq}$  is the equilibrium coefficient matrix,  $\vec{r}$  is a vector of all normal and tangential components of internal forces, and  $\vec{E}$  is a vector of all external forces EF and torques ET.

Following Frick, Van Mele, and Block (2016), the “internal force” at vertex  $i$  of face  $k$  is represented by three components: normal component  $r_{i,k}^n$  (outward with respect to the block centroid) and two tangential components  $r_{i,k}^{t1}$  and  $r_{i,k}^{t2}$ . These three components can also be represented as  $(\vec{e}_k^n \cdot r_{i,k}^n)$ ,  $(\vec{e}_k^{t1} \cdot r_{i,k}^{t1})$ , and  $(\vec{e}_k^{t2} \cdot r_{i,k}^{t2})$ , where  $r_{i,k}^n$ ,  $r_{i,k}^{t1}$ , and  $r_{i,k}^{t2}$  are scalar values and the unit vectors  $\vec{e}_k^n$ ,  $\vec{e}_k^{t1}$ , and  $\vec{e}_k^{t2}$  compose local coordinates for interface  $j$  (Fig. 11b).

The “internal torques” at each vertex  $i$  are also  $[\vec{d}_{i,k} \times r_{i,k}^n]$ ,  $[\vec{d}_{i,k} \times r_{i,k}^{t1}]$ , and  $[\vec{d}_{i,k} \times r_{i,k}^{t2}]$ , where  $\vec{d}_{i,k}$  is the relative position of contact point  $i$  (of interface  $k$ ) with respect to the block centroid. The three expressions can also be written as  $[(\vec{e}_k^n \times \vec{d}_{i,k}^n) \cdot r_{i,k}^n]$ ,  $[(\vec{e}_k^{t1} \times \vec{d}_{i,k}^{t1}) \cdot r_{i,k}^{t1}]$ , and  $[(\vec{e}_k^{t2} \times \vec{d}_{i,k}^{t2}) \cdot r_{i,k}^{t2}]$ .

Then, for a single hexahedron block the equilibrium equation can be formulated as follows:

$$\begin{bmatrix} e_1^{nx} & e_1^{tx} & e_1^{tx} & \dots & e_1^{nx} & e_1^{tx} & e_1^{tx} \\ e_1^{ny} & e_1^{ty} & e_1^{ty} & & e_1^{ny} & e_1^{ty} & e_1^{ty} \\ e_1^{nz} & e_1^{tz} & e_1^{tz} & & e_1^{nz} & e_1^{tz} & e_1^{tz} \\ (e_1^n \times \vec{d}_{1-1})^x & (e_1^t \times \vec{d}_{1-1})^x & (e_1^t \times \vec{d}_{1-1})^x & & (e_1^n \times \vec{d}_{m-1})^x & (e_1^t \times \vec{d}_{m-1})^x & (e_1^t \times \vec{d}_{m-1})^x \\ (e_1^n \times \vec{d}_{1-1})^y & (e_1^t \times \vec{d}_{1-1})^y & (e_1^t \times \vec{d}_{1-1})^y & & (e_1^n \times \vec{d}_{m-1})^y & (e_1^t \times \vec{d}_{m-1})^y & (e_1^t \times \vec{d}_{m-1})^y \\ (e_1^n \times \vec{d}_{1-1})^z & (e_1^t \times \vec{d}_{1-1})^z & (e_1^t \times \vec{d}_{1-1})^z & & (e_1^n \times \vec{d}_{m-1})^z & (e_1^t \times \vec{d}_{m-1})^z & (e_1^t \times \vec{d}_{m-1})^z \end{bmatrix} \dots \begin{bmatrix} e_8^{nx} & e_8^{tx} & e_8^{tx} & \dots & e_8^{nx} & e_8^{tx} & e_8^{tx} \\ e_8^{ny} & e_8^{ty} & e_8^{ty} & & e_8^{ny} & e_8^{ty} & e_8^{ty} \\ e_8^{nz} & e_8^{tz} & e_8^{tz} & & e_8^{nz} & e_8^{tz} & e_8^{tz} \\ (e_8^n \times \vec{d}_{1-8})^x & (e_8^t \times \vec{d}_{1-8})^x & (e_8^t \times \vec{d}_{1-8})^x & & (e_8^n \times \vec{d}_{n-8})^x & (e_8^t \times \vec{d}_{n-8})^x & (e_8^t \times \vec{d}_{n-8})^x \\ (e_8^n \times \vec{d}_{1-8})^y & (e_8^t \times \vec{d}_{1-8})^y & (e_8^t \times \vec{d}_{1-8})^y & & (e_8^n \times \vec{d}_{n-8})^y & (e_8^t \times \vec{d}_{n-8})^y & (e_8^t \times \vec{d}_{n-8})^y \\ (e_8^n \times \vec{d}_{1-8})^z & (e_8^t \times \vec{d}_{1-8})^z & (e_8^t \times \vec{d}_{1-8})^z & & (e_8^n \times \vec{d}_{n-8})^z & (e_8^t \times \vec{d}_{n-8})^z & (e_8^t \times \vec{d}_{n-8})^z \end{bmatrix} \cdot \begin{bmatrix} r_{1-1}^n \\ r_{1-1}^{t1} \\ r_{1-1}^{t2} \\ \vdots \\ r_{m-1}^n \\ r_{m-1}^{t1} \\ r_{m-1}^{t2} \\ \vdots \\ r_{n-8}^n \\ r_{n-8}^{t1} \\ r_{n-8}^{t2} \\ \vdots \\ r_{n-8}^n \\ r_{n-8}^{t1} \\ r_{n-8}^{t2} \end{bmatrix} = \begin{bmatrix} EF^x \\ EF^y \\ EF^z \\ ET^x \\ ET^y \\ ET^z \end{bmatrix}, \quad (3)$$

where interface 1 has  $m$  contact points and interface 8 has  $n$  contact points. As shown,  $C_{eq}$  is formulated so that the orientation and number of connectors can be determined separately for each interface.

For the whole equilibrated system, each interface shared between two blocks is considered as two faces with the same values of  $r^n$ ,  $r^{t1}$ , and  $r^{t2}$  in the opposite directions.  $C_{eq}$  can then be constructed by combining horizontally four submatrices  $C_{uv0}^{sub}$ ,  $C_{uv1}^{sub}$ ,  $C_{uw}^{sub}$ , and  $C_{vw}^{sub}$  of the same height, collecting the coefficients for  $uv0$ ,  $uv1$ ,  $uw$ , and  $vw$  interfaces, respectively, i.e.

$$\begin{bmatrix} uv0_{1,1} & uv0_{1,2} & \dots & uv0_{q,p} \\ b_{1,1} & C_{11} & & \\ b_{1,2} & & C_{22} & \\ \vdots & & & \ddots \\ b_{q,p} & & & C_{p,q \ p,q} \end{bmatrix} = C_{uv0}^{sub}, \quad (4)$$

$$\begin{bmatrix} uv1_{1,1} & uv1_{1,2} & \dots & uv1_{q,p} \\ b_{1,1} & C_{1 \ p,q+1} & & \\ b_{1,2} & & C_{2 \ p,q+2} & \\ \vdots & & & \ddots \\ b_{q,p} & & & C_{p,q \ 2p,q} \end{bmatrix} = C_{uv1}^{sub}, \quad (5)$$

$$\begin{bmatrix} uw_{1,1} & uw_{1,2} & \dots & uw_{q+1,p-1} & uw_{q+1,p} \\ b_{1,1} & C_{1 \ 2p,q+1} & C_{1 \ 2p,q+2} & & \\ b_{1,2} & & C_{2 \ 2p,q+2} & & \\ \vdots & & & \ddots & \\ b_{q,p} & & & C_{p,q \ 3p,q+p-1} & C_{p,q \ 3p,q+p} \end{bmatrix} = C_{uw}^{sub}, \quad (6)$$

$$\begin{bmatrix} vw_{1,1} & \dots & vw_{2,1} & \dots & vw_{q,p} & \dots & vw_{q,p+1} \\ b_{1,1} & C_{1 \ 3p,q+p+1} & \dots & C_{1 \ 3p,q+2p+1} & & & \\ b_{1,2} & & C_{1 \ 3p,q+2p+1} & & & & \\ \vdots & & & \ddots & & & \\ b_{q,p} & & & C_{p,q \ 4p,q+p} & \dots & C_{p,q \ 4p,q+p+q} \end{bmatrix} = C_{vw}^{sub}, \quad (7)$$

where in each  $C_{ij}^{sub}$ ,  $C_{ij}$  is a coefficient submatrix for the  $i$ th interface acting on the  $j$ th block. Equations (4)–(7) show how the interfaces and blocks are arranged within the formulation when the system has  $p$  blocks along  $u$  gridlines and  $q$  blocks along  $v$  gridlines. The empty spaces in the matrices represent zero values. Finally,  $C_{eq}$  is formulated as

$$C_{eq} = \begin{bmatrix} C_{uv0}^{sub} & C_{uv1}^{sub} & C_{uw}^{sub} & C_{vw}^{sub} \end{bmatrix}. \quad (8)$$

When the model is closed along a  $v$  gridline, the first and last rows of  $vw$  faces overlap and can be regarded as interfaces shared between two blocks. To use the coefficient matrix of equation (8) for such a model, a new set of constraints is added, keeping the

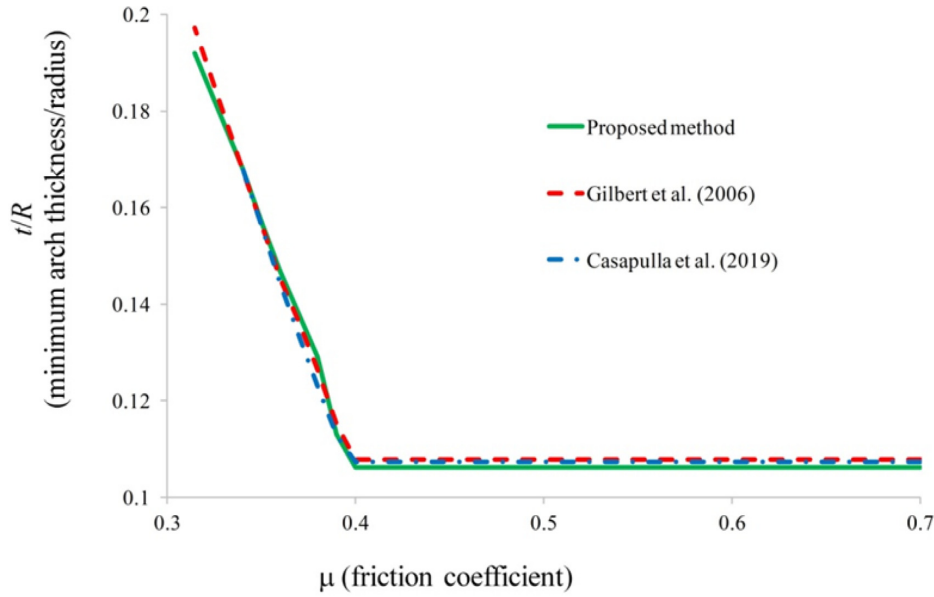


Figure 12: Comparison of the thinnest semicircular arch obtained by the proposed method and by Gilbert, Casapulla, and Ahmed (2006) and Casapulla, Mousavian, and Zarghani (2019).

values of the internal forces on two overlapped faces equal in the opposite directions:

$$R_F^n = -R_L^{t1}, \quad R_F^{t1} = -R_L^{t1}, \quad R_F^{t2} = -R_L^{t2}, \quad (9)$$

where, for vertex  $i$  and every interface  $vw$  of the first (F) and last (L) rows, it is

$$\begin{aligned} R_F^n, R_F^{t1}, R_F^{t2} &= \{r_{i-vw1,1}^n, \dots, r_{i-vw1,p+1}^n\}; \{r_{i-vw1,1}^{t1}, \dots, r_{i-vw1,p+1}^{t1}\}; \{r_{i-vw1,1}^{t2}, \dots, r_{i-vw1,p+1}^{t2}\}, \\ R_L^n, R_L^{t1}, R_L^{t2} &= \{r_{i-vwq,1}^n, \dots, r_{i-vwq,p+1}^n\}; \{r_{i-vwq,1}^{t1}, \dots, r_{i-vwq,p+1}^{t1}\}; \{r_{i-vwq,1}^{t2}, \dots, r_{i-vwq,p+1}^{t2}\}. \end{aligned} \quad (10)$$

As explained earlier, the surface can be converged toward the upper side of the surface, forming a radial grid. In this case, a key unit is considered on the top of the model, whose faces are the last row of the interfaces in  $u$  direction. Also,  $C_{eq}$  is updated by concatenating a row to  $C_{eq}$  to equilibrate the internal forces on the key unit.

The linear system of equation (3) is solved by the least-squares optimization using MATLAB's `lsqmin` method, with linear equality and nonequality constraints. MATLAB is used as a backend connected to the C# environment. Compared to other MATLAB solvers for the linear problem, the result of the least-squares method presents the uniform force distribution.

## 4. Results

This section provides some benchmark examples aimed at presenting different assemblages that can be modeled, analyzed, and modified during the analysis parametrically.

First, the implemented formulation is validated through comparing the thinnest hemispherical dome and semicircular arch with conventional blocks obtained by the developed framework with those obtained by other existing methods. Then, four examples composed of interlocking blocks, respectively, study the influence of (i) the orientation of interfaces and locks; (ii) the orientation of locks and the friction coefficient; (iii) the type of interfaces (conventional and interlocking) and the friction coefficient; and (iv) the concave model option (Section 2.1) and the shear strength on the sliding resistance. The models include open and closed shells along  $v$  directions, subjected to different external forces.

### 4.1. Validation

To validate the formulation, the minimum masonry thicknesses of a semicircular arch and a hemispherical dome obtained by the proposed method are compared to the results obtained by existing methods in the literature, i.e. Gilbert, Casapulla, and Ahmed (2006) and Casapulla, Mousavian, and Zarghani (2019) for the arch (Fig. 12) and Heyman (1995) and Simon and Bagi (2016) for the dome (Fig. 13).

The radius of the semicircular arch CL is 10 m, its depth is 1 m, and it is modeled with 60 blocks under their own weight with 1 N/m<sup>3</sup> density. Blocks have conventional flat interfaces with isotropic sliding resistance. The minimum thickness for different values of friction coefficient is obtained and compared to those obtained by Gilbert, Casapulla, and Ahmed (2006) and Casapulla, Mousavian, and Zarghani (2019) (Fig. 12). The results show that the minimum friction coefficient for a feasible model obtained by the proposed method and by Gilbert, Casapulla, and Ahmed (2006) coincides with each other and is 0.315, while using the method developed by Casapulla, Mousavian, and Zarghani (2019), this value equals 0.332. Applying both the proposed method and the method of Casapulla,



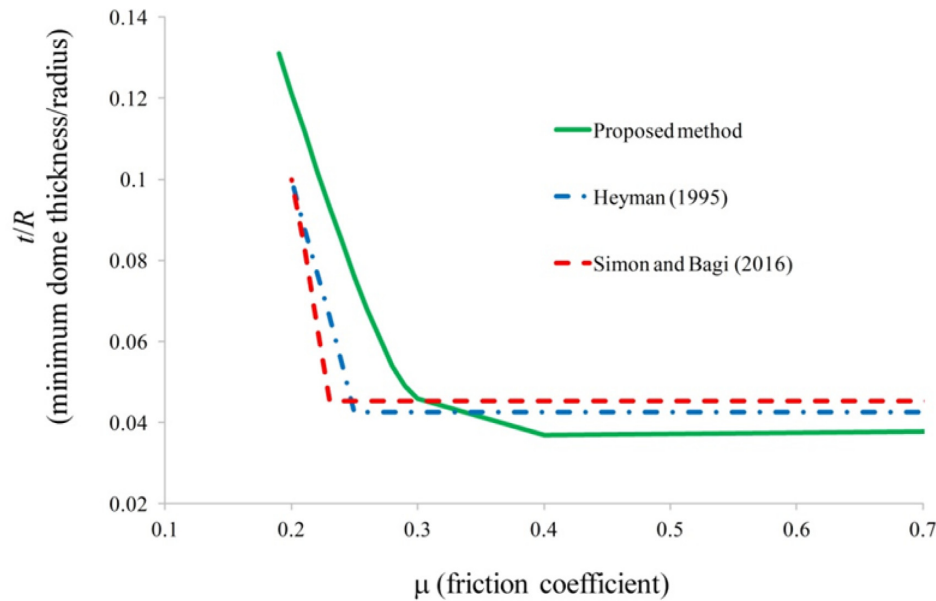


Figure 13: Comparison of the thinnest hemispherical dome obtained by the proposed method and by Heyman (1995) and Simon and Bagi (2016).

Mousavian, and Zarghani (2019), the ratio of the minimum thickness to radius for the arch with friction coefficient more than 0.4 is a constant value, which is 1.078 and 1.063, respectively. This value obtained by the proposed method is a bit lower than the Heyman's solution, which is 1.07 (Heyman, 1995).

The radius of the hemispherical dome CL is 10 m and is modeled with 10 rows and 20 blocks at each row, under their own weight with  $1 \text{ N/m}^3$  density. Blocks have conventional and isotropic flat interfaces. As mentioned in Section 3.2.1, the developed framework can only model a dome with a hole representing a weightless key unit.

For different values of friction coefficient, the minimum thickness of the dome is found and compared to those obtained by Heyman (1995) and Simon and Bagi (2016) (Fig. 13). Using all methods, three types of failure, i.e. pure slide, mixed rocking-sliding, and pure rocking along the meridional direction, can be observed. The results obtained by the proposed method do not coincide with the results obtained by Heyman (1995) and Simon and Bagi (2016). This discrepancy is first due to the introduction of constraints given by equations (9) and (10) to the proposed system of equations when the shell is closed along a  $v$  gridline. The constraints are treated as soft constraints, which can a little reduce the accuracy of the results for the closed shells. Still, the strength of the formulation is the capability of analyzing shells with arbitrary forms and normal or radial gridlines. Furthermore, the existence of a hole on top of the modeled dome changes the results comparing to those obtained by Heyman (1995) and Simon and Bagi (2016). The hole avoids the generation of the 1D interfaces by the proposed framework.

#### 4.2. Example 1

The first example is composed of three blocks with interlocking interfaces depicted in yellow and conventional interfaces shown in white (Fig. 14a and b). The orientation of the interlocking interfaces between two blocks together with the orientation of the locks on those interfaces can be changed parametrically (Fig. 14c and d). The assemblage is under the weight of the blocks, whose density is  $1 \text{ N/m}^3$  (Fig. 14e). Two faces represented in blue in Fig. 14f are the supports, transferring the forces to the ground.

Figure 15 presents the limit stress state for four cases: (i) assemblage with vertical interfaces (yellow faces) and vertical locks; (ii) assemblage with inclined interfaces with  $73^\circ$  angle with respect to the horizontal plane (orange faces) and vertical locks; (iii) assemblage with vertical interfaces and horizontal locks; and (iv) assemblage with inclined interfaces and horizontal locks. The concave model option 2, displayed in Fig. 3, is selected for the analysis. The shear strength is  $10 \text{ N/m}^2$ . The number of locks at each interface is 3.

For the first and second cases, the tangential forces at the interlocking interfaces are along the locks; therefore, the sliding resistance is only governed by the Coulomb's friction law. The vertical interfaces in the first case can avoid sliding when the coefficient friction is more than 0.3, while the friction coefficient for the inclined interfaces of the second model should only be more than 0.06. This result demonstrates that the steeper the interlocking interface, the larger the value for sliding resistance needed to reach the stability. For the third and fourth cases, the tangential forces at the interlocking interfaces are normal to the locks. As a result, the sliding resistance is governed only by shear resistance of the locks and, with friction coefficient equal to 0, the models are stable.

Figure 16 also presents the minimum friction coefficient providing stability for different lock orientations when the interlocking interfaces between the blocks are vertical (blue dash curve) and inclined with  $73^\circ$  angle with respect to the horizontal plane (continuous red curve). Both curves show that changing the locks from a horizontal to vertical orientation, the value of friction coefficient (i.e. the dependence on the frictional resistance of the interfaces) increases.

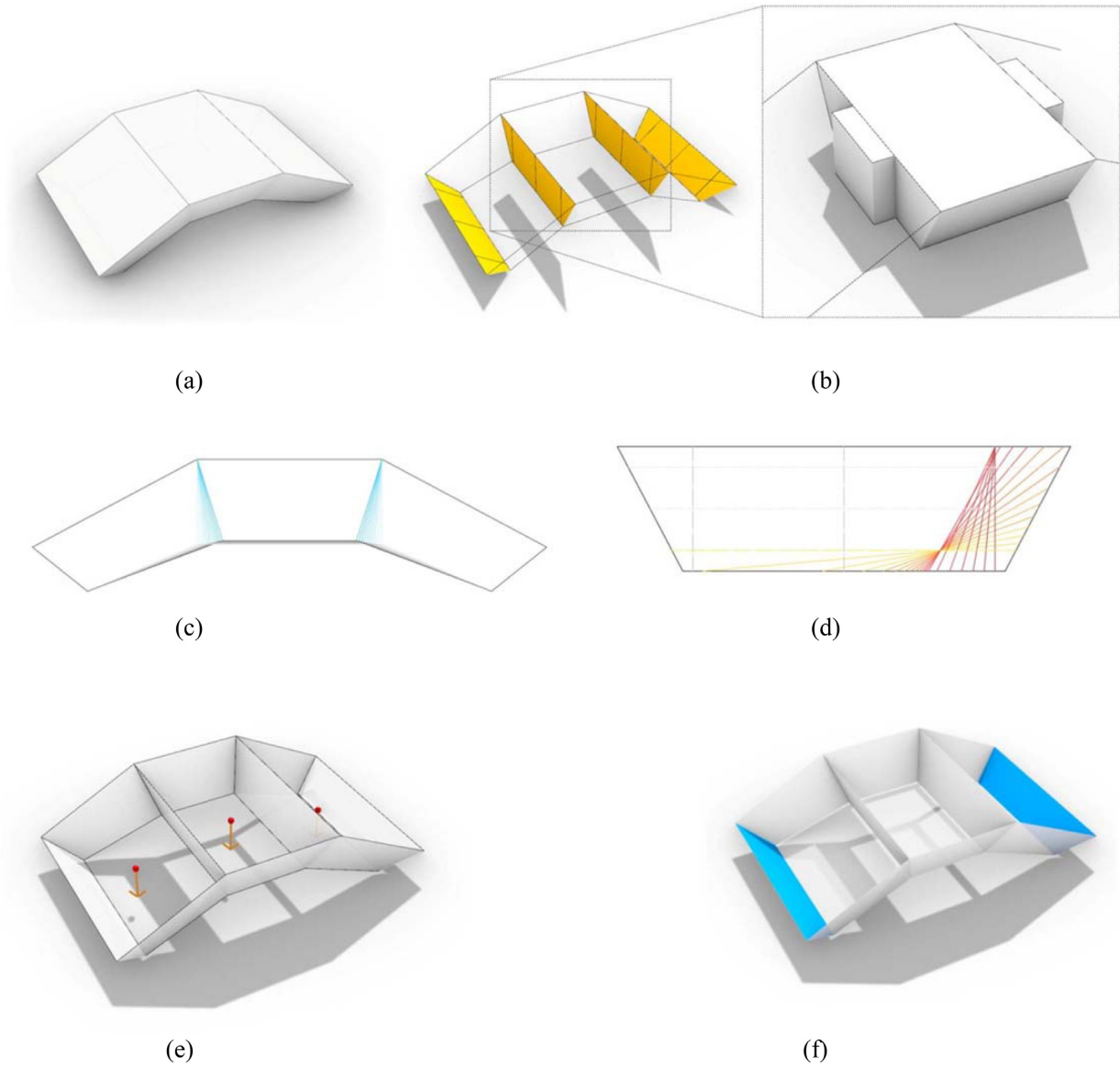


**Figure 14:** (a) Input model of Example 1; (b) interlocking interfaces; (c and d) geometric parameters involved in the shape exploration; (e) loading condition; and (f) boundary condition.

### 4.3. Example 2

The second example is composed of eight blocks with interlocking parallel interfaces. The orientation of the locks on these interfaces changes parametrically (Fig. 17a and b). The external forces imposed on each block are its own weight with  $1 \text{ N/m}^3$  density and a radial force subjected to the block centroid (Fig. 17c). The lower interfaces are considered to be the supports of the assemblage (Fig. 17d). The concave model option 2, displayed in Fig. 3, is selected for the analysis. The shear strength is  $10 \text{ N/m}^2$ .

The limit stress state for three cases is demonstrated in Fig. 18 with lock orientations of  $90^\circ$  (radial),  $45^\circ$ , and  $0^\circ$  (parallel). The friction coefficient for the three models should be more than 0.26, 0.21, and 0.13, respectively. More overall view of the relationship between the lock orientation and the friction coefficient is demonstrated in the graph of Fig. 18. The minimum friction coefficient is needed when the lock orientation is  $10^\circ$ , showing the minimum angle between  $t_2$  direction and the tangential internal force at the contact points (the tangential component of the resultant of the meridional and hoop forces). The dependence of the sliding resistance on the friction coefficient increases by changing the lock orientation from  $30^\circ$  to  $90^\circ$ .

### 4.4. Example 3

The third example is composed of 16 blocks, under their own weight, where density is determined to be  $1 \text{ N/m}^3$  and supporting faces are represented in blue in Fig. 19a and b. The three following cases are studied: (i) all interfaces are conventional flat faces; (ii) the interfaces in one direction are interlocking faces (the number of locks is 3 and the orientation is  $0.8 \text{ rad}$ ) and in the other direction are

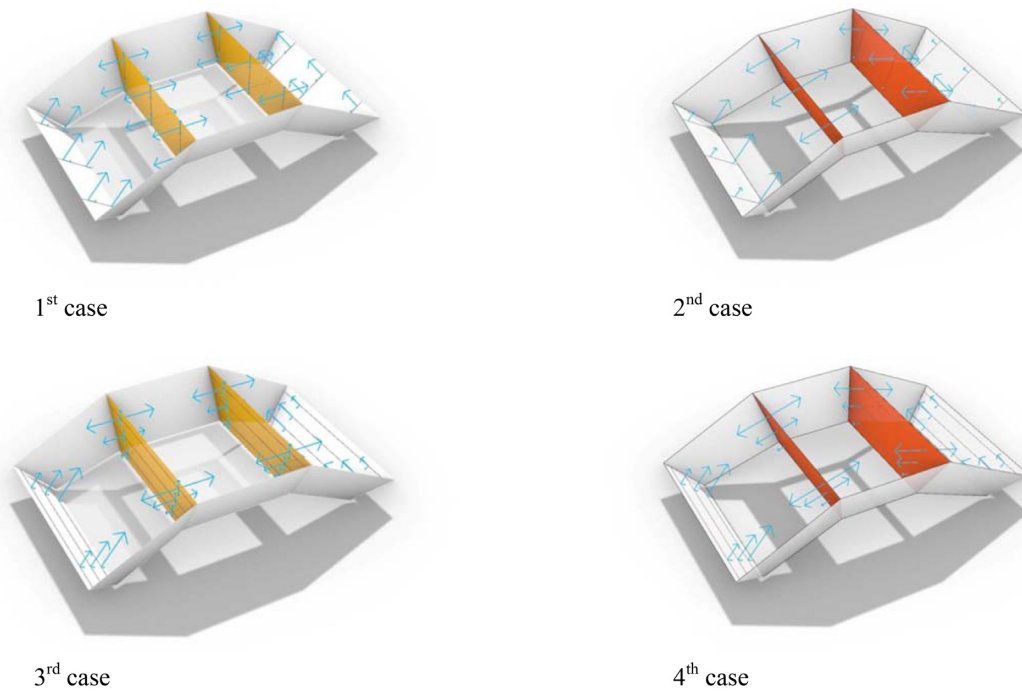


Figure 15: Limit stress state for cases 1–4 of Example 1.

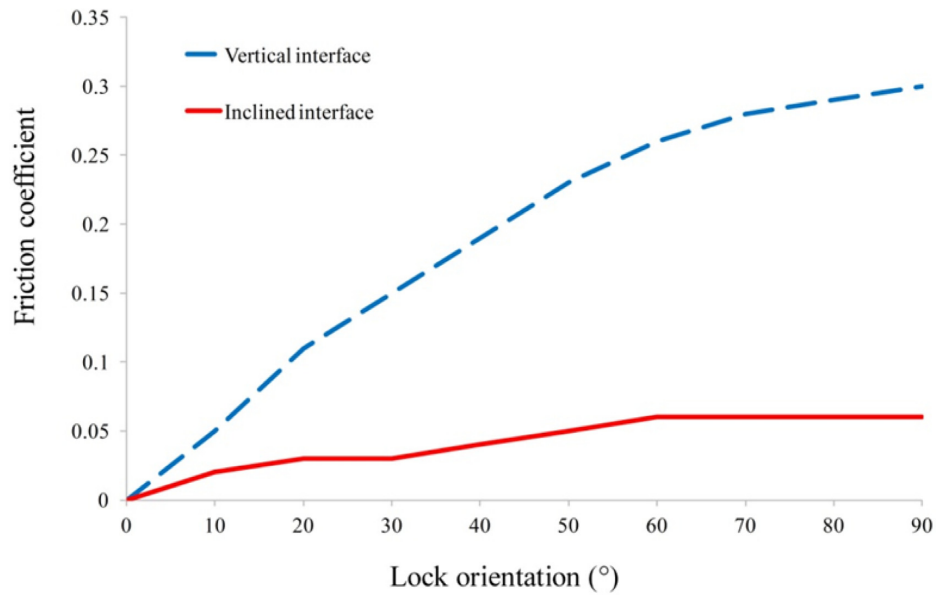
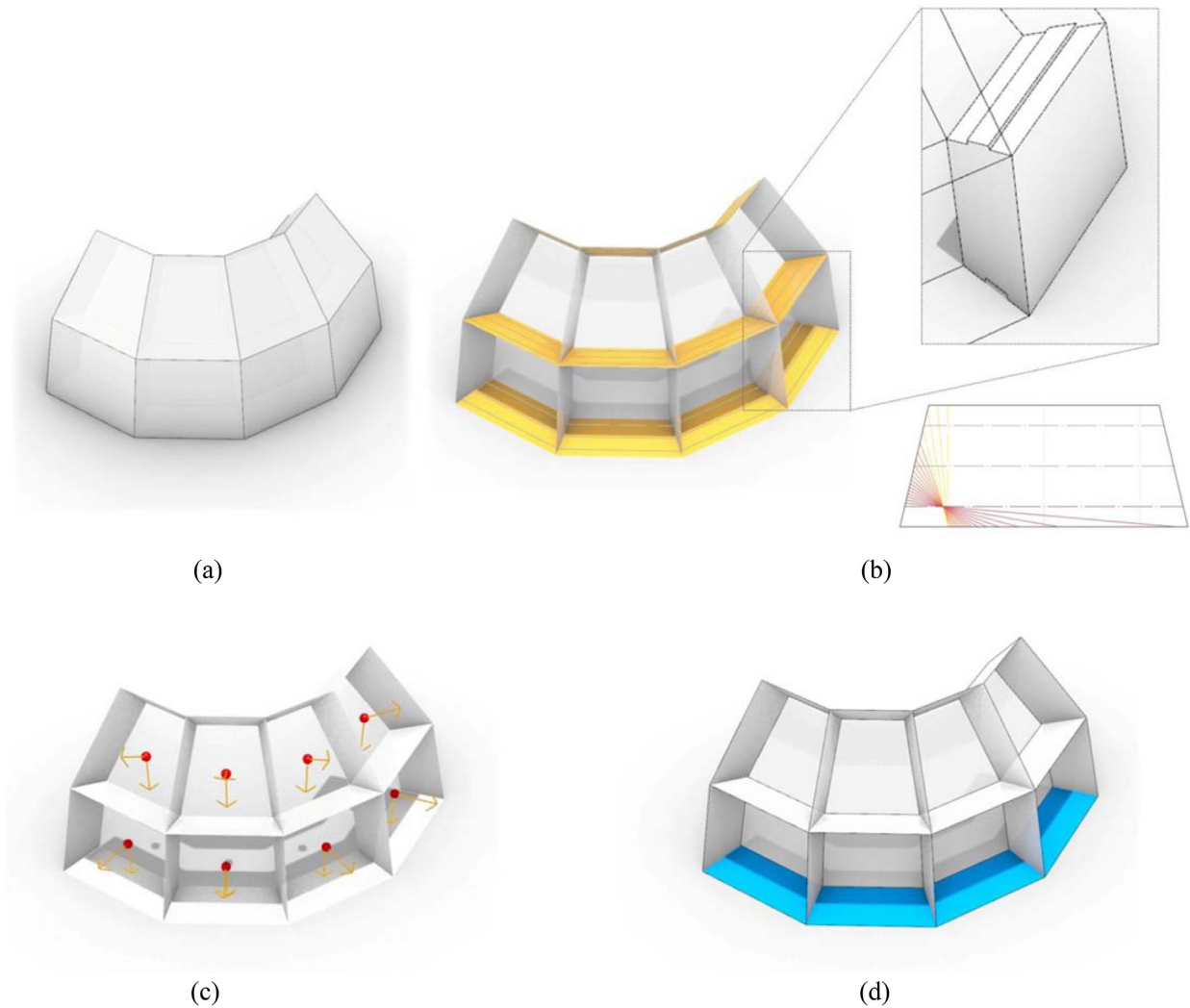


Figure 16: Relationship between the lock orientation and minimum friction coefficient in Example 1.

flat faces; and (iii) the interfaces in two directions are interlocking faces. For the last case, the interfaces in one direction are modeled with three locks at each interface with the orientation of 0.8 rad with respect to the block edge, while the interfaces in the other direction have three locks as well, but the orientation of 2 rad. The concave model option 2, displayed in Fig. 3, is selected for the analysis. The shear strength is 10 N/m<sup>2</sup>.

Figure 20 shows the limit stress state for the three cases in which the minimum friction coefficients for the feasible models are 0.23, 0.11, and 0, respectively. This shows that when the shear strength is large enough, the model whose interfaces are interlocking can be stable with no frictional resistance. Instead, the minimum friction coefficient for such a model with conventional flat interfaces is 0.23.



**Figure 17:** (a) Input model of Example 2; (b) interlocking interfaces and the geometric parameter involved in the shape exploration; (c) loading condition; and (d) boundary condition.

#### 4.5. Example 4

The last example is composed of 80 blocks, arranged radially (closed radial grid). Each block is under its own weight with density of  $1 \text{ N/m}^3$ . The lower interfaces are determined as the supports (blue faces in Fig. 21). The parallel interfaces are interlocking faces with three locks each, while the locks are parallel to the external edge of each block. The friction coefficient is assumed to be 0.7.

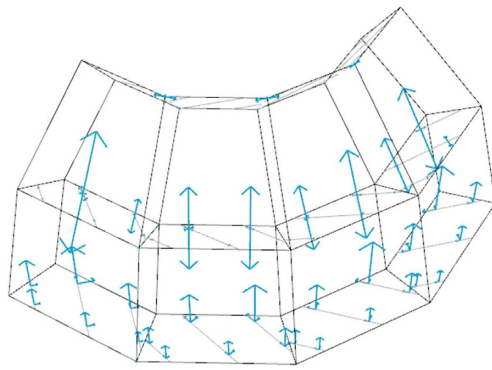
The model is analyzed using the concave model options 1, 2, and 5, displayed in Fig. 3. Using option 1, the shear strength must be more than  $43 \text{ N/m}^2$  for the model to be stable. The computation running time is about 1.9 min, against that required for the previous examples, which is less than a second. Applying option 2, the minimum shear strength is  $49 \text{ N/m}^2$  and computation running time is the same as in the previous case. Using option 5, the lowest feasible value for shear strength is  $43 \text{ N/m}^2$ , and the computation running time is about 4.4 min. The difference of the computation running time among these three cases is due to the use of two control points per lock for the first two options and three control points for the third one. Figure 22 shows the model analyzed by option 1.

### 5. Conclusions

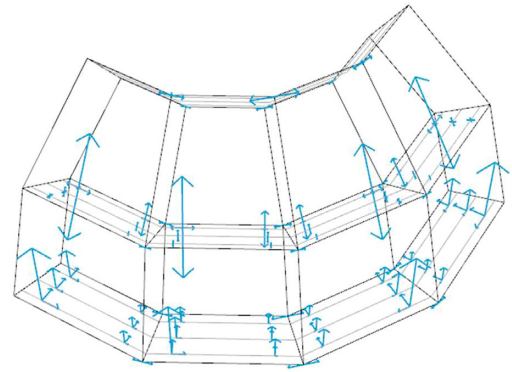
This paper presented a computational framework developed to design structurally feasible assemblages of interlocking blocks, in which the limit analysis was extended to interlocking interfaces with orthotropic sliding resistance. To extend the limit analysis, the concave model was adopted and associated flow rules were considered. Different options for the distribution of the contact points and shear resistance at each point were proposed, and the torsion–shear interaction for them was tested.

The extended limit analysis was adopted to design and analyze single-layer shells having cuboid blocks with corrugated interfaces, assembled using stack bond pattern. The developed formulation is capable of being extended to multilayer assemblages with different bonding patterns, though.

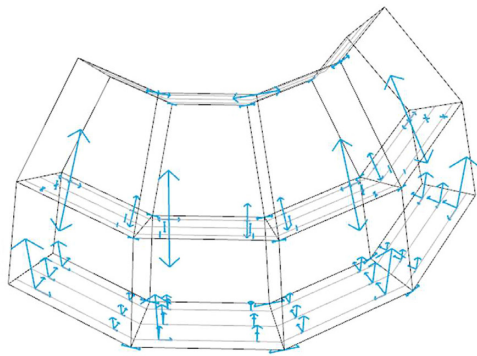




Lock orientation: 90 degrees  
Friction coefficient: 0.28



Lock orientation: 45 degrees  
Friction coefficient: 0.21



Lock orientation: 0 degree  
Friction coefficient: 0.13

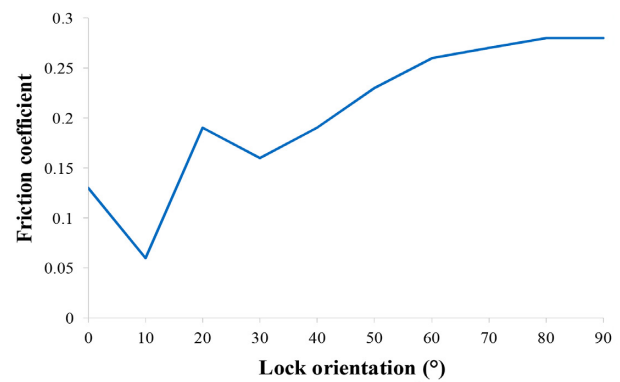


**Figure 18:** Limit stress state for the models with lock orientation 90° (radial), 45°, and 0° (parallel). The graph shows the relationship between the lock orientation and the friction coefficient.

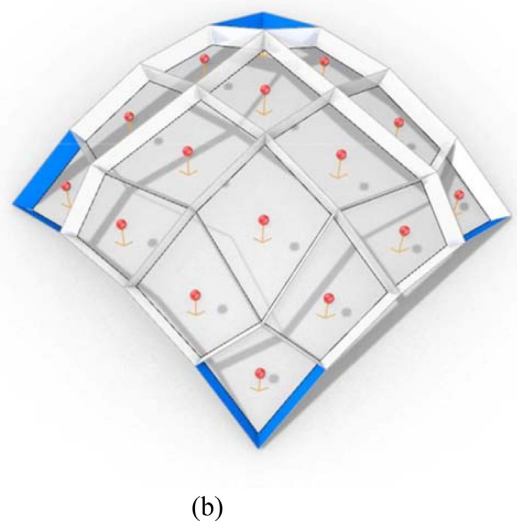
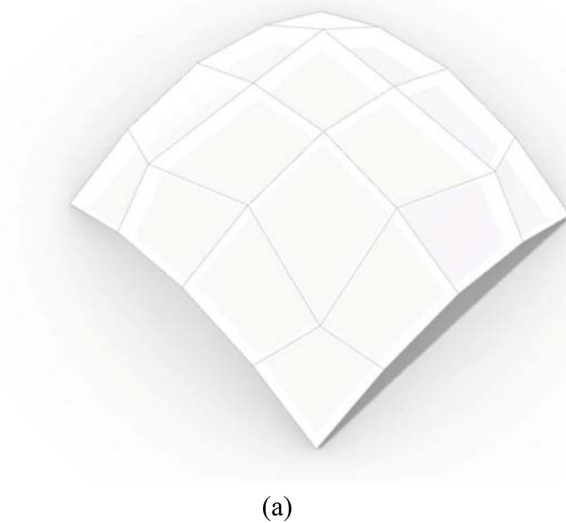


**Figure 19:** (a) Input model of Example 3 and (b) loading and boundary conditions.

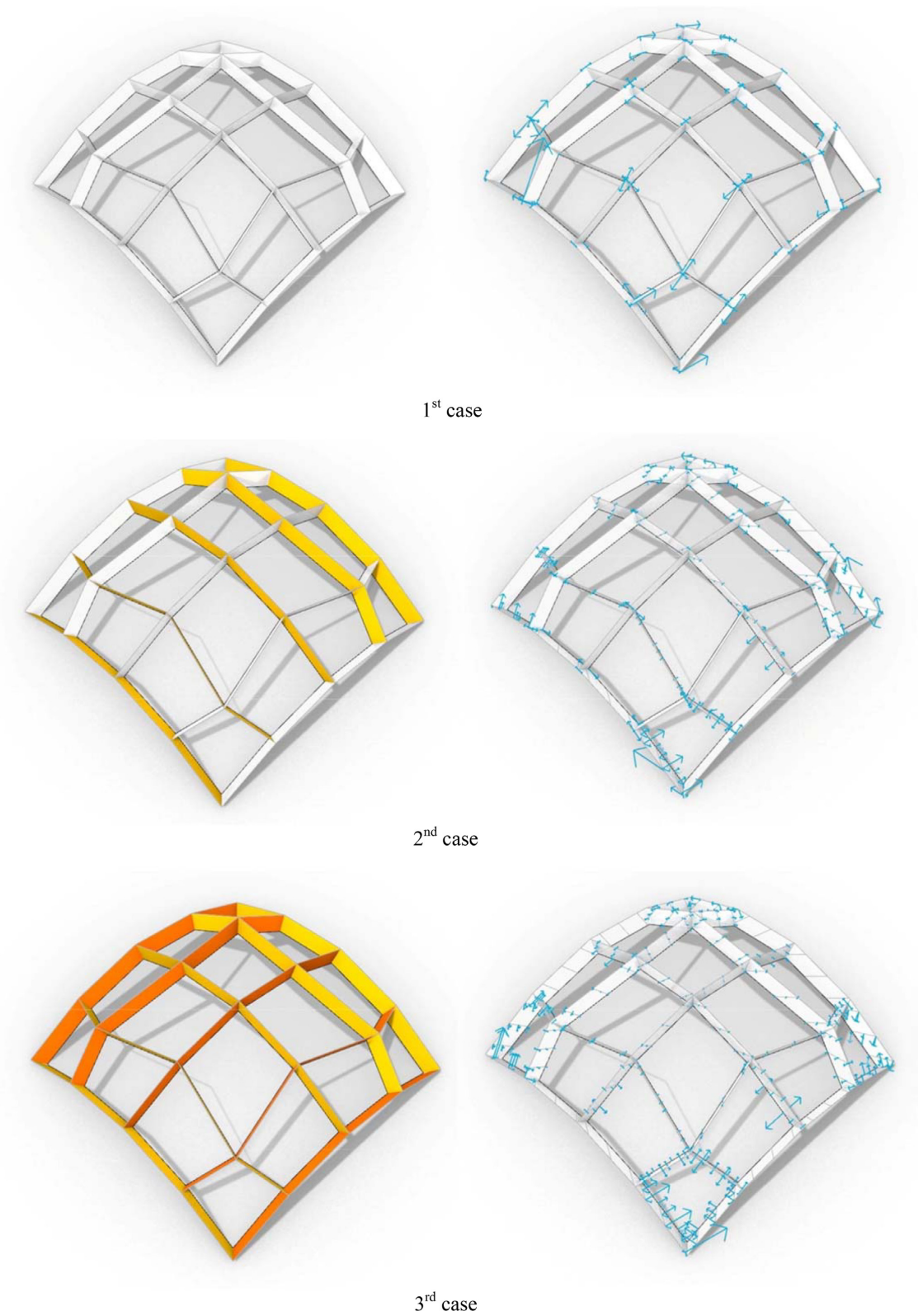


Figure 20: Limit stress state for cases 1–3 of Example 3.

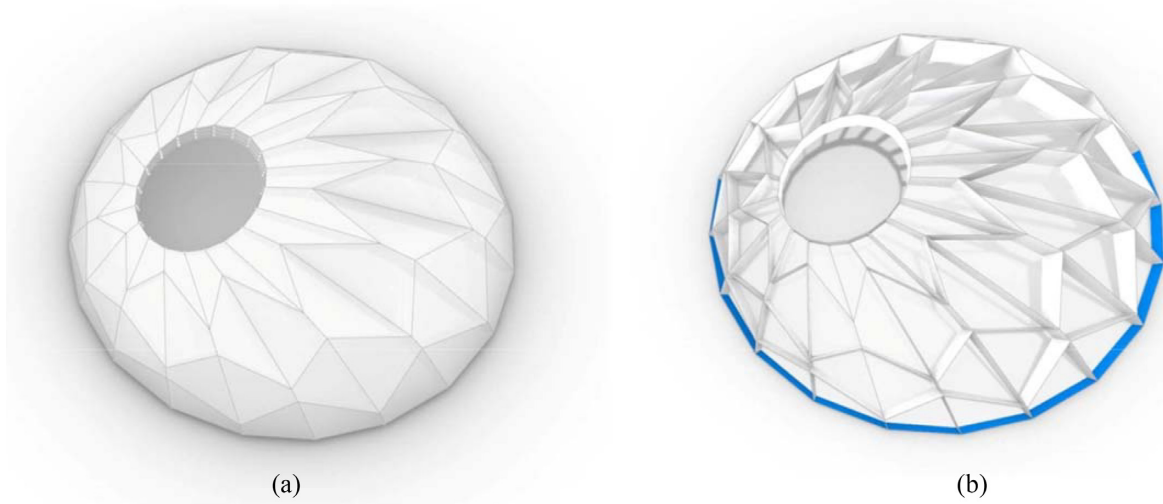


Figure 21: (a) Input model of Example 4 and (b) boundary condition.

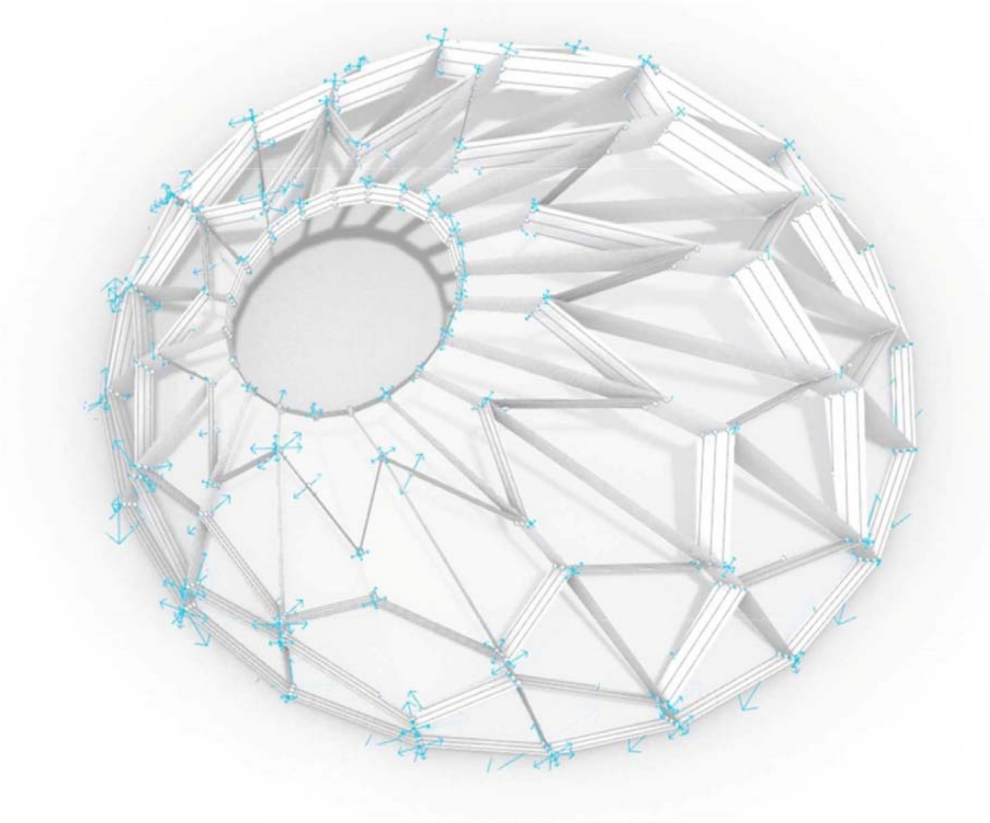


Figure 22: Limit stress state of Example 4 analyzed using the concave model option 1 displayed in Fig. 3.

The designer can tune the geometry of the block assemblage and their interlocking interfaces parametrically, to remove the structural infeasibility. The functionality of the framework, including the parametric adjustment of geometry of the interlocking blocks, was demonstrated through several examples. In the future, this geometry adjustment will be carried out automatically through developing an optimization procedure minimizing the infeasibility.

Furthermore, in future work, the torsion–shear behavior of locks will be studied in more detail using experimental investigations, and limit analysis will be extended to different geometries of interlocking interfaces, also considering nonassociated flow rules.



## Acknowledgements

This project has received funding from the European Union's Horizon 2020 research and innovation programme under the Marie Skłodowska-Curie Grant Agreement No. 791235. It reflects only the authors' view and the Agency is not responsible for any use that may be made of the information it contains.

## Conflict of interest statement

Declarations of interest: none.

## References

- Akbarzadeh, M., Van Mele, T., & Block, P. (2014). Compression-only form finding through finite subdivision of the force polygon. In *Proceedings of Annual Symposium of the International Association for Shell and Spatial Structures (IASS2014)* (Vol. 2014, No. 16, pp. 1–7), Brasilia, Brazil.
- Akbarzadeh, M., Van Mele, T., & Block, P. (2015). On the equilibrium of funicular polyhedral frames and convex polyhedral force diagrams. *Computer-Aided Design*, 63, 118–128.
- Ali, M., Gultom, R. J., & Chouw, N. (2012). Capacity of innovative interlocking blocks under monotonic loading. *Construction and Building Materials*, 37, 812–821.
- Bagi, K. (2014). When Heyman's safe theorem of rigid block systems fails: Non-Heymanian collapse modes of masonry structures. *International Journal of Solids and Structures*, 51, 2696–2705.
- Block, P. (2009). *Thrust network analysis: Exploring three-dimensional equilibrium* (PhD thesis). Massachusetts Institute of Technology, Cambridge, MA.
- Block, P., & Lachauer, L. (2011). Closest-fit, compression-only solutions for free form shells. In *Proceedings of the IABSE-IASS Symposium* (pp. 1–8).
- Bui, T. T., Limam, A., Sarhosis, V., & Hjiar, M. (2017). Discrete element modelling of the in-plane and out-of-plane behavior of dry-joint masonry wall constructions. *Engineering Structures*, 136, 277–294.
- Cannizzaro, F., Pantò, B., Caddemi, S., & Calò, I. (2018). A discrete macro-element method (DMEM) for the nonlinear structural assessment of masonry arches. *Engineering Structures*, 168, 243–256.
- Casapulla, C., & Argiento, L.U. (2018). In-plane frictional resistances in dry block masonry walls and rocking-sliding failure modes revisited and experimentally validated. *Composites Part B: Engineering*, 132, 197–213.
- Casapulla, C., Giresini, L., Argiento, L.U., & Maione, A. (2019). Nonlinear static and dynamic analysis of rocking masonry corners using rigid macro-block modelling. *International Journal of Structural Stability and Dynamics*, 19(11), 1950137.
- Casapulla, C., & Maione, A. (2018). Modelling the dry-contact interface of rigid blocks under torsion and combined loadings: Concavity vs. convexity formulation. *International Journal of Non-Linear Mechanics*, 99, 86–96.
- Casapulla, C., Mousavian, E., & Zarghani, M. (2019). A digital tool to design structurally feasible semi-circular masonry arches composed of interlocking blocks. *Computers and Structures*, 221, 111–126.
- Casapulla, C., & Portioli, F. (2015). Experimental and analytical investigation on the frictional contact behavior of 3D masonry block assemblages. *Construction and Building Materials*, 78, 126–143.
- Chisari, C., Macorini, L., Amadio, C., & Izzuddin, B. A. (2018). Identification of mesoscale model parameters for brick-masonry. *International Journal of Solids and Structures*, 146, 224–240.
- D'Ayala, D. F., & Casapulla, C. (2001). Limit state analysis of hemispherical domes with finite friction. In *Proceedings of the 3rd International Conference on Structural Analysis of Historical Constructions (SAHC01)* (pp. 617–626), Guimaraes, Portugal.
- D'Ayala, D. F., & Tomasoni, E. (2011). Three-dimensional analysis of masonry vaults using limit state analysis with finite friction. *International Journal of Architectural Heritage*, 5(2), 140–171.
- Dyskin, A. V., Estrin, Y., & Pasternak, E. (2019). Topological interlocking materials. In Y. Estrin, Y. Bréchet, J. Dunlop, & P. Fratzl (Eds.), *Architected materials in nature and engineering* (pp. 23–49). Berlin, Germany: Springer.
- Dyskin, A. V., Pasternak, E., & Estrin, Y. (2012). Mortarless structures based on topological interlocking. *Frontiers of Structural and Civil Engineering*, 6(2), 188–197.
- Fang, D., & Mueller, C.T. (2018). Joinery connections in timber frames: analytical and experimental explorations of structural behavior. In *Proceedings of Annual Symposium of the International Association for Shell and Spatial Structures (IASS2018)* (pp. 1–8).
- Fernando, S., Weir, S., Reinhardt, D., & Hannouch, A. (2019). Towards a multi-criteria framework for stereotomy—Workflows for subtractive fabrication in complex geometries. *Journal of Computational Design and Engineering*, 6(3), 468–478.
- Frick, U., Van Mele, T., & Block, P. (2015). Decomposing three-dimensional shapes into self-supporting, discrete-element assemblies. In M. R. Thomsen, M. Tamke, C. Gengnagel, B. Faircloth, & F. Scheurer (Eds.), *Modelling behavior* (pp. 187–201). Cham, Switzerland: Springer.
- Frick, U., Van Mele, T., & Block, P. (2016). Data management and modelling of complex interfaces in imperfect discrete-element assemblies. In *Proceedings of Annual Symposium of the International Association for Shell and Spatial Structures (IASS2016)* (Vol. 2016, No. 17, pp. 1–9), Tokyo, Japan.
- Gilbert, M., Casapulla, C., & Ahmed, H.M. (2006). Limit analysis of masonry block structures with non-associative frictional joints using linear programming. *Computers and Structures*, 84(13–14), 873–887.
- Giresini, L., Sassu, M., & Sorrentino, L. (2018). In situ free-vibration tests on unrestrained and restrained rocking masonry walls. *Earthquake Engineering and Structural Dynamics*, 47(15), 3006–3025.
- Giresini, L., Solarino, F., Paganelli, O., Oliveira, D.V., & Froli, M. (2019). One-sided rocking analysis of corner mechanisms in masonry structures: Influence of geometry, energy dissipation, boundary conditions. *Soil Dynamics and Earthquake Engineering*, 123, 357–370.



- Harvey, W. J. (1988). Application of the mechanism analysis to masonry arches. *Structural Engineer*, 66(5), 77–84.
- Heyman, J. (1995). *The stone skeleton: Structural engineering of masonry architecture*, Cambridge, UK: Cambridge University Press.
- Hossain, M. A., Totoev, Y., & Masia, M. J. (2016). Friction on mortar-less joints in semi interlocking masonry. In *Proceedings of 16th International Brick and Block Masonry Conference (IBMAC 2016)*(pp. 1635–1643), Padova, Italy.
- Kooharian, A. (1952). Limit analysis of voussoir (segmental) and concrete arches. *Journal of American Concrete Institute*, 4(4), 317–328.
- Lee, J., Van Mele, T., & Block, P. (2016). Form-finding explorations through geometric transformations and modifications of force polyhedrons. In *Proceedings of IASS Annual Symposia*(Vol. 2016, No. 15, pp. 1–10). International Association for Shell and Spatial Structures (IASS).
- Lee, J., Van Mele, T., & Block, P. (2018). Disjointed force polyhedra. *Computer-Aided Design*, 99, 11–28.
- Lemos, J. V. (2017). Contact representation in rigid block models of masonry. *International Journal of Masonry Research and Innovation*, 2(4), 321–334.
- Li, T., & Atamturktur, S. (2013). Fidelity and robustness of detailed micromodeling, simplified micromodeling, and macromodeling techniques for a masonry dome. *Journal of Performance of Constructed Facilities*, 28(3), 480–490.
- Liu, H., Liu, P., Lin, K., & Zhao, S. (2016). Cyclic behavior of mortarless brick joints with different interlocking shapes. *Materials*, 9(3), 166.
- Livesley, R. K. (1978). Limit analysis of structures formed from rigid blocks. *International Journal for Numerical Methods in Engineering*, 12(12), 1853–1871.
- Livesley, R. K. (1992). A computational model for the limit analysis of three-dimensional masonry structures. *Meccanica*, 27(3), 161–172.
- Lourenço, P. B., Rots, J. G., & Blaauwendraad, J. (1995). Two approaches for the analysis of masonry structures: Micro and macro-modeling. *Heron*, 40(4), 1–28.
- O'Dwyer, D. (1999). Funicular analysis of masonry vaults. *Computers and Structures*, 73(1–5), 187–197.
- Olmati, P., Gkoumas, K., & Bontempi, F. (2019). Simplified FEM modelling for the collapse assessment of a masonry vault. *Frattura ed Integrità Strutturale*, 13(47), 141–149.
- Portioli, F., Casapulla, C., Gilbert, M., & Cascini, L. (2014). Limit analysis of 3D masonry block structures with non-associative frictional joints using cone programming. *Computers and Structures*, 143, 108–121.
- Rippmann, M. (2016). *Funicular shell design: Geometric approaches to form finding and fabrication of discrete funicular structures* (PhD thesis). ETH-Zürich, Zürich.
- Sassu, M., De Falco, A., Giresini, L., & Puppio, M. (2016). Structural solutions for low-cost bamboo frames: Experimental tests and constructive assessments. *Materials*, 9(5), 346.
- Sassu, M., Giresini, L., Bonannini, E., & Puppio, M. L. (2016). On the use of vibro-compressed units with bio-natural aggregate, *Buildings*, 6(3), 40.
- Simon, J., & Bagi, K. (2016). Discrete element analysis of the minimum thickness of oval masonry domes. *International Journal of Architectural Heritage*, 10(4), 457–475.
- Sossou, G., Demoly, F., Montavon, G., & Gomes, S. (2018). An additive manufacturing oriented design approach to mechanical assemblies. *Journal of Computational Design and Engineering*, 5(1), 3–18.
- Totoev, Y. (2015). Design procedure for semi interlocking masonry. *Journal of Civil Engineering and Architecture*, 9, 517–525.
- Van Mele, T., & Block, P. (2014). Algebraic graph statics. *Computer-Aided Design*, 53, 104–116.
- Wang, Z., Song, P., & Pauly, M. (2018). DESIA: A general framework for designing interlocking assemblies. *ACM Transactions on Graphics*, 37(6), 1–14.
- Whiting, E., Ochsendorf, J., & Durand, F. (2009). Procedural modeling of structurally-sound masonry buildings. *ACM Transactions on Graphics*, 28(5), 1–9.
- Zboinska, M. A. (2019). Influence of a hybrid digital toolset on the creative behaviors of designers in early-stage design. *Journal of Computational Design and Engineering*, 6(4), 675–692.